Frost flowers and sea-salt aerosols over seasonal sea-ice areas in north-western Greenland during winter–spring

Keiichiro Hara[1], Sumito Matoba[2], Motohiro Hirabayashi[3], and Tetsuhide Yamasaki[4]

[1] Department of Earth System Science, Faculty of Science, Fukuoka University
[2] Institute of Low Temperature Science, Hokkaido University
[3] National Institute of Polar Research, Tokyo, Japan
[4] Avangnaq, Osaka, Japan

Correspondence to: K. Hara (harakei@fukuoka-u.ac.jp)

Abstract. Sea-salts and halogens in aerosols, frost flowers and brine play an important role in atmospheric chemistry in polar regions. Simultaneous sampling and observations of frost flowers, brine, and aerosol particles were conducted around Siorapaluk in north-western Greenland during December 2013 – March 2014. Results show that water-soluble frost flower and brine constituents were sea salts (e.g., Na^+, Cl^-, Mg^{2+}, and Br^-). Concentration factors of sea-salt constituents of frost flowers and brine relative to seawater were 1.14–3.67. Sea-salt enrichments of Mg^{2+}, K^+, Ca^{2+}, and halogens (Cl^-, Br^-, and I) in frost flowers were associated with sea-salt fractionation by precipitation of mirabilite and hydrohalite. Aerosol number concentrations, particularly in coarse mode, were increased considerably by release from the sea-ice surface under strong wind conditions. Sulphate depletion by sea-salt fractionation was found to be slight in sea-salt aerosols because of heterogeneous SO_4^{2-} formation on sea-salt particles. However, coarse and fine sea-salt particles were found to be rich in Mg. Strong Mg enrichment might be more likely to proceed in fine sea-salt particles. Mg-rich sea-salt particles might be released from the sea-ice surface and frost flowers. Mirabilite-like and ikaite-like particles were identified only in aerosol samples collected near new sea-ice areas.

1 Introduction

Frost flowers are fragile ice crystals containing brine and sea salt. They appear often during winter–spring in polar regions on the surface of new and young sea ice. Frost flowers play an important role as an interface among the atmosphere, sea ice, and ocean. Key conditions for formation and growth of frost flowers are (1) a cold atmosphere (below -15 °C) and (2) weak–calm winds (Perovich and Richter-Menge, 1994; Martin et al., 1995, 1996; Style and Worster, 2009; Roscoe et al., 2011). Particularly, vertical gradients of temperature and relative humidity near the sea-ice surface are crucially important for the appearance of frost flowers. Frost flowers can be formed by condensation of water vapour on nodules on new and young sea ice. From results of earlier studies (e.g., Domine et al., 2005; Douglas et al., 2012), water vapour is supplied from the atmosphere, with sublimation and/or evaporation provided by a warm sea-ice surface. For a strong vertical gradient of air temperature above the sea-ice surface, the vertical gradients engender supersaturation of water vapour near the sea-ice surface;

then they induce condensation of water vapour (i.e., formation of frost flowers). The concentrated seawater (i.e. brine) is present on new and young sea ice. Therefore, brine with high salinity migrates upwardly and gradually on frost flowers (Perovich and Richter-Menge, 1994; Martin et al., 1996; Roscoe et al., 2011). Under cold conditions, solutes with lower solubility in brine can be precipitated in and on sea ice and frost flowers depending on the temperature. Previous investigations

5 (e.g., Marion, 1999; Koop et al., 2000; Diekmann et al., 2008, 2010; Geilfus et al., 2013) reported that several salts can be precipitated at -2.2 °C (ikaite, $CaCO_3 \cdot 2H_2O$), -8.2 °C (mirabilite, $Na_2SO_4 \cdot 10H_2O$), -15 °C (gypsum, $CaSO_4$), -22.9 °C (hydrohalite, $NaCl \cdot 2H_2O$), -28°C ($NaBr \cdot 5H_2O$), -33 °C (sylvite, KCl), -36°C ($MgCl_2 \cdot 12H_2O$), and -53.8 °C (antarcticite, $CaCl_2 \cdot 6H_2O$). The salt precipitation at lower temperatures causes changes to sea-salt ratios in brine and frost flowers, known as *sea-salt fractionation*.

Frost flowers have a fine and fragile structure. Sea salts on and in frost flowers can be released easily to the atmosphere through their fracture under strong wind conditions. Because of the lower number density of aerosol particles in polar regions, especially in Antarctic regions, emission of sea-salt particles from sea-ice areas is an important aerosol source during winter–spring (e.g., Wagenbach et al., 1998; Rankin et al., 2000; Hara et al., 2004, 2011, 2012, 2013). Actually, sea-salt particles

15 released from sea-ice areas are dispersed from the boundary layer to the free troposphere (up to ca. 4 km) over Syowa Station, Antarctica through vertical motion by cyclone activity (Hara et al., 2014), and into the interior (Dome F Station and Concordia Station) of the Antarctic continent (Hara et al., 2004; Udisti et al., 2012). Vertical transport of the sea-salt particles originating from sea ice can act as a supply of cloud condensation nuclei (CCN) and ice nuclei (IN) in the upper boundary layer – free troposphere. Because of the horizontal transport of sea-salt particles into the Antarctic plateau, the Na^+ records in ice cores

20 taken in the inland area have been used recently as a proxy of the sea-ice extent (e.g., Wolff et al., 2003, 2006).

As described above, sea-salt fractionation proceeds on new and young sea ice. For that reason, sea-salt ratios in sea-salt particles (or aerosols) released from sea-ice areas differ from those of bulk seawater ratio (Hara et al., 2012, 2013). For instance, Mg-rich sea-salt particles and aerosol particles containing $MgCl_2$ and $MgSO_4$ were identified to a remarkable degree at Syowa

25 Station during winter–spring because precipitation of mirabilite and hydrohalite engender Mg-enrichment in sea-salt particles (Hara et al., 2012, 2013). Because the relative humidity of Mg-salt deliquescence, such as that of $MgCl_2$, is lower than that of NaCl (e.g., Kelly and Wexler, 2005), sea-salt fractionation can engender modification of aerosol hygroscopicity, which is closely related to phase transformation, heterogeneous reactions, and abilities of cloud condensation nuclei and ice nuclei. In addition to sea-salt fractionation, sea-salt ratios in frost flowers and aerosols can be altered gradually by heterogeneous

30 reactions in a process known as *sea-salt modification*. Furthermore, frost flowers have large specific surface area: 63–299 cm^2 g^{-1} (mean, 162 cm^2 g^{-1}) at Hudson Bay, Canada (Obbard et al., 2009) and 185 (+80, -50) cm^2 g^{-1} at Barrow, Alaska (Domine et al., 2005). Because of that larger surface area, earlier studies have discussed the potential of frost flowers as reaction sites (e.g., Kaleschke et al., 2004, references in Abbatt et al., 2012). Sea-salt modification in sea-salt aerosols, and sea salts in and on frost flowers and sea ice can act as potential sources of gaseous reactive species. For instance, gaseous reactive halogen

species (e.g., Br_2, HOBr, Br, and BrO) induce depletion of ozone and mercury near the surface in both polar regions during the polar sunrise (Barrie et al., 1988; Schroeder et al., 1998; Foster et al., 2001; Ebinghaus et al., 2002). According to laboratory experiments conducted by Koop et al. (2000), Br^- can be enriched in frost flowers by sea-salt fractionation. Reportedly, Br^- enrichment occurs in frost flowers at Barrow, Alaska (Douglas et al., 2012), and slightly in the Weddell Sea, Antarctica (Rankin

5 et al., 2002). However, results of some earlier studies have indicated non-significant Br^- enrichment in frost flowers at Barrow and Hudson Bay (Alvarez-Aviles et al., 2008; Obbard et al., 2009). Therefore, many issues persist with respect to sea-salt and halogen chemistry of aerosols and frost flowers. They demand further measurement and discussion.

To elucidate the atmospheric impact of fractionated sea-salt particles, and their relation between sea-salt particles in the
10 atmosphere and frost flowers on sea ice, one must ascertain their (1) chemical properties (e.g., concentrations, ratios, and pH) of frost flowers and brine, and (2) the physical and chemical properties of aerosols (e.g., size distribution, constituents, and mixing states) above seasonal sea ice with frost flowers. In spite of the importance, simultaneous observations and measurements of aerosols and frost flowers over seasonal ice areas with frost flower appearance have not been reported for polar regions, although sampling and observations of frost flowers have been conducted in the Arctic (e.g., Alvaraz-Aviles et
15 al., 2008; Douglas et al., 2012) and Antarctica (Rankin et al., 2000, 2002). This study aims to obtain knowledge related to sea-salt constituents and their ratios of frost flowers, brine and aerosols, and abundance of the fractionated sea-salt particles over seasonal sea ice from simultaneous measurements and sampling of aerosols, frost flowers, and brine around north-western Greenland during winter–spring.

2 Samples and Analysis

20 ### 2.1 Sampling sites and conditions

Figure 1 shows that simultaneous observations of frost flowers, brine, seawater, and aerosols were conducted on new and young sea-ice area in Robertson fjord near Siorapaluk in north-western Greenland from mid-December, 2013 through mid-March, 2014. In the fjord, the open sea surface appears during summer. Sea ice forms gradually from October, 2013. Sea ice flowed out several times from the fjord by the action of sea tides, heaving, and strong winds (Fig. 1) before and during the
25 measurements in this study. Therefore, sea ice of different ages (new – very old) was present in the fjord in front of the fjord of Siorapaluk. We chose Sites I–III (new – young sea ice; less than 1 cm - ca. 35 cm thickness) as sampling sites of aerosols, frost flowers, brine, and seawater. Site I was approximately 2 km distant from Siorapaluk. The sea ice on Site I had flowed during 10–12 February, 2014 (shown by red broken line); then it refroze. Site II had younger sea ice than Site I did. Before several days to a week, an open-lead appeared around Site II. Thereafter, new sea ice was formed. The refrozen lead width
30 was 2–6 m. Site III was close to the sea-ice edge. The sea surface appeared on approximately 1 March by sea-ice breakage and strong winds (shown by the blue broken line). Then, new sea ice formed again. This new sea ice at Site III (less than 1 cm thickness) was a few days old when we made direct samplings. New sea ice formed gradually on the sea surface off Site III

(photographs, Fig. 1). We accessed sampling sites with frost flowers on foot and by dog sledge from Siorapaluk. Sampling sites are shown in Fig. 1.

2.2 Sampling of frost flowers, brine, and seawater

Sampling of frost flowers, brine, and seawater was conducted from 20 February, 2014 through 3 March, 2014 on sea ice near

5   Siorapaluk. Frost flowers were taken from the sea-ice surface using a clean stainless steel shovel. The pieces of frost flowers were moved into polyethylene bags (Whirl-pak; Nasco). From one site, frost flowers of several forms were collected in a single sample. Brine samples were collected by shaving off a thin layer of the sea-ice surface into polyethylene bags (Whirl-pak; Nasco) using a stainless-steel shovel. Seawater samples were collected in polypropylene bottles using a dropper from a crack in the sea ice or a hole we made in the sea ice. All samples were melted at ambient temperature. Concentration of H^+ (i.e., pH)

10 of the liquid sample was measured using a portable pH meter (B-212; Horiba Instruments Ltd.). Then residue of the sample was transferred to polypropylene bottles. After the bottled liquid samples were transported to Japan, all were kept frozen in a cold room until chemical analyses were conducted.

2.3 Aerosol sampling and measurements

Aerosol measurements and direct sampling were conducted over seasonal sea ice around Siorapaluk, Greenland from 17

15 December, 2013 through 7 March, 2014. Aerosol number concentrations were measured using a portable optical particle counter (OPC, KR12A; Rion Co. Ltd.). The measurable size range was D_p >0.3, >0.5, >0.7, >1.0, >2.0, and >5.0 μm. The OPC packed in an insulator box was set at ca. 1 m above the sea-ice surface by a tripod.   Aerosol number concentrations were recorded every 23–25 s, corresponding to 1 L air sucking, during aerosol direct sampling. Details of OPC measurements were described in Hara et al. (2014).

Direct aerosol sampling was made using a two-stage aerosol impactor. Carbon-coated collodion thin films supported by a Ni micro-grid (square-300 mesh; Veco Co.) were used as sample substrates in this study. The cut-off diameters (aerodynamic diameter) of the impactor were 2.0 and 0.2 μm at a flow rate of ca. 1.2 L min^{-1}. The impactor was set at ca. 1 m above the seasonal sea-ice surface, similar to OPC measurement. Direct aerosol sampling was conducted for 10-15 min depending on

25 aerosol number concentrations. Aerosol samples were kept in polyethylene capsules immediately after aerosol measurements and sampling. The polyethylene capsules with aerosol samples were packed into polyethylene bags with a zipper. All bags with aerosol samples were put into an airtight box together with a desiccant (Nisso-Dry M; Nisso Fine Co. Ltd.) until analysis to prevent humidification that can engender morphology change and efficient chemical reactions, as described by Hara et al. (2002, 2005, 2013, 2014).

Meteorological data (air temperature, relative humidity, air pressure, wind direction, and wind speed) were measured using an auto-weather station (HOBO U30-NRC Weather Station; Onset Computer Corp.), which was set on the coast near Siorapaluk

and ca. 1 km away from the village. Meteorological data were recorded to data logger of the auto-weather station in time resolution of 5 min. A thermorecorder (TR-7Wf; T and D Corp.) and thermosensor (TR1106; T and D Corp.) were used for measurements of temperature of seawater, slash layer (brine) on sea ice, base of frost flowers on slush layer, and the atmosphere above the top of the frost flowers.

2.4 Sample analysis

2.4.1 Analysis of frost flower, brine, and seawater

Re-frozen samples of frost flower, brine, snow, and seawater were melted in ambient temperature before chemical analyses. Concentrations of ion species (Na^+, K^+, Mg^{2+}, Ca^{2+}, Cl^-, NO_3^- and SO_4^{2-}) were measured using ion chromatography (ICS 2100; Thermo Fisher Scientific) after 10^3-fold dilution by ultrapure water. A guard column (IonPac CG12; Thermo Fisher Scientific), column (IonPac CS12; Thermo Fisher Scientific) and a 20 mM CH_3SO_3H eluent for the cation measurement, and Guard column (IonPac AG14; Thermo Fisher Scientific), column (IonPac AS14; Thermo Fisher Scientific) and 3.5 mM NaOH eluent were used for the anion measurement. Concentrations of Br^- in frost flower and brine were measured using an ion chromatograph-mass spectrometer (IC-MS) after 10^6-fold dilution using ultra-pure water. Ionic contents in samples were separated using ion chromatography with a guard column (IonPac AG11-HC; Thermo Fisher Scientific), a column (IonPac AS11-HC; Thermo Fisher Scientific) and gradient KOH eluent (4–36 mM), and were injected into a mass spectrometer (6100 series single quadrupole LC/MS; Agilent Technologies). The detection limit of Br^- in IC-MS was 0.9 ng L^{-1}. Iodine concentrations in frost flower and brine were measured after 10^3-fold dilution using ultra-pure water using an inductively coupled plasma-mass spectrometer (ICP-MS: 7700 series single quadrupole ICP-MS, Agilent Technologies). The RF power and flow of carrier Ar gas were 1550 W and 0.80 L min^{-1}, respectively, in ICP-MS analysis. The detection limit of iodine was 17 ng L^{-1} in this study. Samples of frost flower and brine were injected into ICP-MS after melt. Therefore, iodide and iodate were not divided in this study. Details of analytical procedures of IC-MS will be described elsewhere by Hirabayashi et al. (preparation for publication). We calculated concentration factors (CF-X) with concentrations of chemical species (X) in samples divided by concentration of X in seawater to evaluate concentration processes of the chemical species during formation and aging of frost flowers.

2.4.2 Analysis of individual aerosol particles

Individual aerosol particles on the sample substrate were observed and analysed for this study using a scanning electron microscope equipped with an energy dispersive X ray spectrometer (SEM-EDX, Quanta FEG-200F, FEI, XL30; EDAX Inc.). The analytical conditions were 20 kV accelerating voltage and 30 s counting time. Details of analytical procedures were in accordance with Hara et al. (2013, 2014). We analysed 1261 particles in coarse mode (mean: 41 particles a sample) and 6337 particles in fine mode (mean: 192 particles a sample). Most aerosol-sampled areas on the substrates were analysed in coarse

mode in this study. Although we attempted to analyse as many coarse particles as possible, the lower aerosol number concentrations in coarse mode limit the number of the analysed aerosol particles in this study.

3. Results and Discussion

3.1 Meteorological conditions during the campaign

Figure 2 depicts time variations of air temperature, relative humidity and wind speed during our measurement. The air temperature was -34.2 – 1.8 °C. Colder conditions below -20°C occurred in the day of year (DOY) = 47.5–58.6 (February 17–28, 2014) during our intensive sampling and observations of aerosols and frost flowers. Because of the cyclone approach, several strong wind events occurred during the campaign. Particularly strong winds in DOY = 39.7–41.2 (9–11 February) caused breaks and outflows of sea ice from the front of Siorapaluk (ca. 1 km away). Then, the seawater started refreezing immediately after recovery of the weather. Sea ice off Siorapaluk (ca. 5–6 km away) was broken and flowed out again off Siorapaluk by storm conditions on DOY = 58.9–60.3 (February 28 – March 1). Sea ice was formed after recovery of weather conditions. Frost flowers appeared on the new sea ice in both cases.

3.2 Conditions of frost flowers

Sea ice conditions where frost flowers formed can be categorized as three types in this study: young ice (Site I), younger ice in refrozen leads between young ice (Site II), and new sea ice (Site III). Figure 3 depicts photographs of frost flowers observed at Site I, which was categorized as young ice (Fig. 3a) on 20 February. The sea-ice surface was partly covered with thin snow and frost flowers were formed patchily on the ice surface without snow cover. The surface of the sea ice underneath frost flowers was wet by brine (sherbet-like). Figure 3b presents a close up photograph of frost flowers observed on 22 February at the same site on 20 February. Salt crystals deposited on the branches of frost flower crystals were identified. Figure 3c shows frost flowers observed at Site II (Fig. 1). The surface of sea ice underneath frost flowers was wet by brine. Figure 3d shows frost flowers observed at site III (Fig. 1) on 4 March. The site was close to the edge of sea ice to open water. The frost flower diameter was approximately 5 mm. The surface of the sea ice was covered with brine water (Fig. 3e). The frost flower crystals were partially submerged in the brine water.

3.3 Concentrations of sea salts in frost flowers and brine on sea ice

Figure 4 depicts relations among the respective constituents of frost flowers, brine, and seawater found in this study. Concentrations of Na^+ in frost flowers and brine were 48–154 mmol L^{-1}, which greatly exceeded the seawater concentration. The concentration factors of Na^+ (CF_{Na}) in frost flowers and brine were 1.14–3.67, which roughly approximated values reported by previous studies (e.g., Rankin et al., 2002; Alvarez-Aviles et al., 2008). High correlation among constituents was identified in both frost flowers and brine, as follows.

Frost flowers:

$[Cl^-] = 1.302 [Na^+] + 2.158 (R^2 = 0.969)$

$[Br^-] = 0.0022 [Na^+] + 0.025 (R^2 = 0.910)$

5    $[I^-] = 1.17 \times 10^{-6} [Na^+] + 5.867 \times 10^{-4} (R^2 = 0.791)$

$[Mg^{2+}] = 0.122 [Na^+] - 0.761 (R^2 = 0.982)$

$[K^+] = 0.023 [Na^+] - 0.063 (R^2 = 0.988)$

$[Ca^{2+}] = 0.023 [Na^+] - 0.019 (R^2 = 0.996)$

10   Brine:

$[Cl^-] = 1.421 [Na^+] - 21.35 (R^2 = 0.964)$

$[Br^-] = 0.002 [Na^+] + 0.06 (R^2 = 0.962)$

$[I^-] = 1.10 \times 10^{-6} [Na^+] + 3.25 \times 10^{-5} (R^2 = 0.842)$

$[Mg^{2+}] = 0.114 [Na^+] - 0.8267 (R^2 = 0.982)$

15    $[K^+] = 0.022 [Na^+] - 0.140 (R^2 = 0.988)$

$[Ca^{2+}] = 0.021 [Na^+] - 0.023 (R^2 = 0.972)$

High correlation coefficients imply strongly that the constituents are sea salts (derived from seawater). With mirabilite precipitation in sea-ice formation at temperatures lower than ca. -9 °C, molar ratios of the respective constituents relative to

20   Na^+ can be raised gradually (e.g., Hara et al., 2012). The slopes in each regression line (Fig. 4) and the molar ratios in frost flowers were larger than the seawater ratio found in this study. Therefore, sea-salt fractionation might occur in frost flowers. Moreover, the slopes in frost flowers were higher than those in brine except Cl^-. However, the slopes of Mg^{2+}-Na^+, K^+-Na^+, and Ca^{2+}-Na^+ in brine were slightly higher than the seawater ratio. Figure 4 and Table 1 show that the molar ratios in frost flowers and brine varied depending on sampling sites, circumstances such as temperature, and the age of frost flowers (details

25   are discussed later herein). Therefore, preferential sea-salt enrichment might be promoted considerably in frost flowers and slightly or negligibly in brine. The molar ratios in frost flowers resembled the ratios found by previous studies of frost flowers and aerosols (Rankin et al., 2002; Douglass et al., 2012; Hara et al., 2012). The Br^-/Na^+ ratios found from previous investigations, however, were varied considerably at frost flower sampling sites (Rankin et al., 2002; Alvarez-Aviles et al., 2008; Douglass et al., 2012). Br^- enrichment in frost flowers was observed in this study and previous studies conducted at

30   Barrow, Alaska by Douglass et al. (2012) and in the Weddell Sea, Antarctica by Rankin et al. (2002), although Alvarez-Aviles et al. (2008) and Obbard et al. (2009) reported that Br^- was not enriched respectively in frost flowers (similar to seawater ratio) at Barrow, Alaska and at Hudson Bay, Canada. This difference might result from conditions of solar radiation and sea-salt

fractionation processes depending on air temperature and temperature at the sea-ice surface. Details are presented in a later section (3–4).

Precipitation of salts such as mirabilite and hydrohalite depend on temperature (Marion et al., 1999; Koop et al., 2000).
5   Therefore, we attempted to compare relations of respective sea salts to Cl^- and Mg^{2+} (Supplementary, Figures S1 and S2). Relations among Mg^{2+}, K^+, Ca^{2+}, and Cl^- in frost flowers well matched those in brine. The molar ratios to Cl^- were not changed by mirabilite precipitation without Cl^- loss by heterogeneous reactions. Considering that the first step of precipitation of Na salt is mirabilite precipitation approximately at -9 °C, the coincidence of the relations of among Mg^{2+}, K^+, Ca^{2+}, and Cl^- suggests that enrichment of Mg^{2+}, K^+, and Ca^{2+} in frost flowers was driven mainly by mirabilite precipitation. When hydrohalite
10   precipitation occurs under colder conditions, the molar ratios to Cl^- can rise in brine and frost flowers. As presented in Table 1, the molar ratios to Cl^- in some brine samples markedly exceeded the seawater ratios. Therefore, sea-salt fractionation by hydrohalite might be promoted in some samples of brine and frost flowers. By contrast, frost flowers were more likely to be richer in Br^- and I^- than in Cl^- and Mg^{2+} (Table 1, Figs. S1 and S2). Minimum air temperatures (-34.1 °C) during measurements were higher than temperatures of $MgCl_2 \bullet 6H_2O$ precipitation (-36 °C). Therefore, $MgCl_2 \bullet 6H_2O$ precipitation might not occur
15   during the measurements, although precipitation of mirabilite and hydrohalite can occur. Consequently, enrichment of Br^- and I^- in frost flowers might derive from sea-salt fractionation to a greater degree than precipitation of mirabilite and hydrohalite. A molecular dynamics (MD) simulation conducted by Jungwirth and Tobias (2001) predicted considerable surface enhancement of Br^- and I^- in alkaline halide solutions. If Br^- and I^- are enhanced also at the brine surface, then this surface enhancement and sea-salt fractionation by precipitation of mirabilite and hydrohalite might engender enrichment of Br^- and I^-
20   in frost flowers.

3.4 Aging of frost flower and brine on sea ice

Figure 5 presents variations of CF_{Na} and molar ratio of SO_4^{2-}/Cl^- in frost flowers at each sampling Site I. As described above, aged frost flowers, young frost flowers, and fresh frost flowers were collected respectively at Site I, Site II, and Site III. CF_{Na} of all samples exceeded 1.0, even on new ice at Site III, indicating that concentrated brine was excluded from sea ice to the
25   sea-ice surface during sea-ice formation before formation of frost flowers (Fig. 5a). CF_{Na} of frost flower at Site III area was lower than that at Sites I and II. Therefore, processes for highly concentrated sea salts might proceed with (1) the growth of sea ice and frost flowers, and (2) drying process by evaporation of water molecules from the sea-ice surface and frost flowers. Some parts of frost flowers and the sea ice in Site I showed low values of CF_{Na} because of dilution by fresh snow cover after formation of sea ice and frost flowers.

Molar ratios SO_4^{2-}/Cl^- in frost flowers at Sites I and II (Fig. 5b) were considerably lower than the seawater ratio. This change of SO_4^{2-}/Cl^- ratios might be attributed to sea-salt fractionation by sulphate depletion (i.e., mirabilite precipitation). By contrast, SO_4^{2-}/Cl^- ratios at Site III were similar to the seawater ratio. The distribution of SO_4^{2-}/Cl^- ratios implies strongly that sea-salt

fractionation (e.g., mirabilite formation) occurs to a non-significant degree on new sea-ice at Site III. Non-significant sea-salt fractionation might result from the following likelihood: (1) warm condition (air temperature, approx. -15 °C), (2) reduction of cooling near the sea-ice surface by heat conduction from seawater to the sea-ice surface, and (3) insufficient concentration of sea salts to be precipitated in brine. After storm conditions, the sea surface started re-freezing at air temperatures of

5 approximately -15°C on 1 March. Considering that a strong vertical gradient of temperature near the sea-ice surface was necessary for frost flower formation (Perovich and Richter-Menge, 1994; Martin et al., 1995, 1996; Style and Worster, 2009; Roscoe et al., 2011), lower air temperatures might be necessary to reach the temperature of mirabilite precipitation near the sea-ice surface. Therefore, temperatures near the sea-ice surface might not be likely to fall to the temperature of mirabilite precipitation.

To compare changes of sea-salt constituents with aging of frost flowers, we attempted to monitor the sea-salt constituents of frost flowers and brines at Site I on 20–28 February, 2014. Figure 6 depicts short-term variations of air temperatures measured by AWS (T_{AWS}), air temperature above frost flowers (T_{air}, ca. 10 cm above brine/sea-ice surface), temperature at bases of frost flowers (T_{FF}) and molar ratios of sea salts (SO_4^{2-}/Na^+, SO_4^{2-}/Cl^-, Br^-/Cl^-, I^-/Cl^-, Mg^{2+}/Cl^-, K^+/Cl^-, and Ca^{2+}/Cl^-) in frost flowers

15 and brine. Unfortunately, we did not measure T_{air} and T_{FF} on 20–22 February. Sea-salt ratios in brines at Site I were distributed along with seawater ratios. They varied non-significantly, although the ratios of Mg^{2+}/Cl^-, K^+/Cl^-, and Ca^{2+}/Cl^- were slightly higher than their respective seawater ratios. In contrast to the ratios in brines, molar ratios of SO_4^{2-}/Na^+ and SO_4^{2-}/Cl^- in frost flowers dropped greatly relative to seawater ratios. T_{AWS} on 20–28 February was lower than the temperature for mirabilite formation (ca. -9°C). In addition, T_{FF} was -18.9 – -21.3 °C on 24–28 February. Therefore, the lower ratios of SO_4^{2-}/Na^+ and

20 SO_4^{2-}/Cl^- in frost flowers might be attributed to mirabilite formation. With sulphate depletion, ratios of Mg^{2+}/Cl^-, K^+/Cl^-, and Ca^{2+}/Cl^- increased from 20 February to 24 February. In spite of the non-significant change of molar ratios of SO_4^{2-}/Na^+ and SO_4^{2-}/Cl^- in frost flowers on 26 February, other sea-salt ratios (Mg^{2+}/Cl^-, K^+/Cl^-, and Ca^{2+}/Cl^-) increased remarkably. Figure 6a shows that T_{AWS} and T_{air} had been lower than -25 °C since 23 February. T_{FF} was lower than -18.9 °C in 24–28 February (minimum, -21.3 °C). Considering the temperature for hydrohalite precipitation (ca. -22 °C), this drastic change of the sea-salt

25 ratios on 26 February might be associated with hydrohalite precipitation. In contrast to T_{FF}, T_{air} increased slightly on 26–27 February, and then increased greatly on 28 February – 1 March. In spite of the slight increase of T_{AWS} and T_{air}, T_{FF} tended to decrease slightly on 24–27 February. This decrease of T_{FF} might be attributed to reduction of heat conduction by sea-ice growth (larger thickness). Consequently, the sea-ice thickness might be a fundamentally important factor for sea-salt fractionation on sea ice, in addition to T_{air}. It is noteworthy that molar ratios in frost flowers cannot change if sea-salt fractionations such as

30 mirabilite and hydrohalite precipitation occur on frost flowers after brine migration onto frost flowers. Whether mirabilite and hydrohalite were precipitated on frost flowers or not, the total amount (mass) of precipitated salts and sea salts in residual brine did not change without liberation by heterogeneous reactions. Although halides (Cl^-, Br^-, and I^-) can be liberated from frost flowers, Mg^{2+}, K^+, and Ca^{2+} cannot be liberated by heterogeneous reactions. Suggesting (1) considerable change of the molar

ratios in frost flowers, (2) non-significant change of those in brine, and (3) T_{FF} close to ca. -21 °C, precipitation of mirabilite and hydrohalite might be driven near the surface of brine on the sea ice. Then, the residual brine might be migrated vertically onto frost flowers. Because of the strong vertical gradient of the air temperature near the surface of the sea ice and frost flowers, subsequent sea-salt fractionation can proceed near the tip of frost flowers under colder conditions. In this study, the vertical

5   gradient of sea-salt fractionation on frost flowers could not be identified from bulk analysis of sea-salt constituents.

Molar ratios of Br^-/Cl^- and I/Cl^- in frost flowers were higher than the seawater ratio (values in literature) and brine (Figs. 6d–6e). As described above, Br^- and I were enriched in frost flowers at Site I. Although ratios of Mg^{2+}/Cl^-, K^+/Cl^-, and Ca^{2+}/Cl^- increased drastically on 26–28 February, increases in ratios of Br^-/Cl^- were slight; those of I/Cl^- were not clear. To elucidate

10   this feature, the following likelihood should be considered: (1) reduction of Br^- and I enrichment by precipitation of salts containing Br^- and I, and (2) liberation of Br^- and I from frost flowers through heterogeneous reactions. According to laboratory experiments by Koop et al. (2000), $NaBr\bullet5H_2O$ can be precipitated at -28 °C. In the periods on 20–28 February, air temperatures reached occasionally below -28 °C. T_{FF}, however, did not reach to -28 °C, as depicted in Fig. 6a. Therefore, $NaBr\bullet5H_2O$ might not be precipitated in brine or around bases of frost flowers. $NaBr\bullet5H_2O$ can be precipitated on the fringe

15   of frost flowers if the air temperature around the top of frost flowers reached ca. -28 °C. If so, then we cannot catch evidence of the Br^- enrichment in this case because of bulk analysis in this study. Because of slightly higher of Br^-/Cl^- ratio on 27 February than the ratios on 22–26 February, Br^- might be enriched by hydrohalite. No report in the relevant literature describes of discusses a study of precipitation of iodine salts in sea salts. Next, we attempt to estimate the molar ratios of Br^-/Cl^- and I/Cl^- in frost flowers using the ratios of Mg^{2+}/Cl^-, Br^-/Cl^- and I/Cl^- on 22–26 February, assuming that hydrohalite was not precipitated

20   yet on 22–26 February, and that Br^- and I did not liberate from frost flowers through heterogeneous reactions. When the molar ratios on 22–26 February changed by the assumptions above, the molar ratios of Br^-/Cl^- and I/Cl^- in frost flowers after hydrohalite precipitation were estimated respectively as 0.00214 and 1.82×10^{-6}. The estimated ratios were higher than the ratios of Br^-/Cl^- (0.00206) and I/Cl^- (1.562×10^{-6}) in frost flowers on 27 February. This difference strongly implies the likelihood that Br^- and I were liberated from frost flowers. Br^- and I can be released from frost flowers through the following

25   heterogeneous reactions (Thompson and Zafiriou, 1983; Mochida et al., 2000; Carpenter, 2003; Simpson et al., 2007; Saiz-Lopez et al., 2015).

$$Br^- + O_3 \rightarrow BrO^- + O_2 \qquad\qquad (R1)$$
$$BrO^- + H^+ \rightarrow HOBr \qquad\qquad (R2)$$
30     $$HOBr + Br^- + H^+ \rightarrow Br_2 + H_2O \qquad\qquad (R3)$$
$$HOI + Br^- + H^+ \rightarrow IBr + H_2O \qquad\qquad (R4)$$
$$I^- + H_2O_2 \rightarrow HOI + OH^- \qquad\qquad (R5)$$
$$HOI + I^- + H^+ \rightarrow I_2 + H_2O \qquad\qquad (R6)$$

I⁻ + O₃ + H₂O → HOI + O₂ + OH   (R7)

$$I^- + O_3 + H_2O \rightarrow HOI + O_2 + OH \qquad (R7)$$
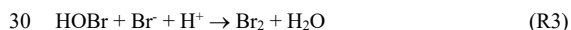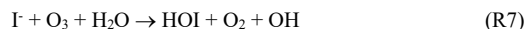
Reactions of R1, R2, and R7 can proceed under nighttime conditions. Other reactions, however, are enhanced under conditions with solar radiation because HOBr and HOI can be formed efficiently through atmospheric photochemical reactions. Frost

5   flowers at Site I had been exposed to direct solar radiation since 18 February, 2014, although it had been dusk at noon since early February. Therefore, the heterogeneous loss of Br⁻ and I⁻ from frost flowers can engender reduction of enrichment of Br⁻ and I⁻ after hydrohalite precipitation in frost flowers. Considering the short-term features of Br⁻/Cl⁻ and I⁻/Cl⁻ in frost flowers, heterogeneous I⁻ loss appears likely to occur from frost flowers relative to heterogeneous Br⁻ loss. Therefore, frost flowers with sea-salt enrichment might play a role as one source of atmospheric reactive halogen species via heterogeneous reactions (e.g.,

10   R1–R7).

3.5 Morphology of sea-salt particles

Figure 7 depicts SEM images of aerosol particles collected above the sea-ice area with frost flowers. Most coarse aerosol particles collected on 1 March 2014 had structures with cuboid-crystal like materials (bright colour in SEM image) and non-crystal materials (gray – dark gray color in SEM image) around the cuboid-crystal like materials. Furthermore, most aerosol

15   particles had stains around the particles. The presence of stains is direct evidence that the aerosol particles had a liquid surface in the atmosphere. In other words, the particles were deliquescent in the atmosphere. Na, Cl, and Mg were detected in aerosol particles of this type. Therefore, the particles might be identified as sea-salt particles. Strong peaks of Na and Cl were identified from cuboid-crystal like materials, whereas strong peaks of minor sea salts such as Mg, K, and S were also obtained from non-crystal materials (see *Supplementary Information*, Fig. S3). Depending on the amount (mass) of sea salts and water in a sea-

20   salt particle, salts with lower solubility can exist in a state with a solid core. In SEM observations, however, aerosol particles were exposed to high vacuum conditions. They dried up. The localization of each sea salt in a particle might proceed in a high vacuum chamber. Therefore, it is noteworthy that the salt distribution in an SEM image differed from the state in the ambient atmosphere. Details of elemental compositions are presented in the next section.

3.6 Elemental compositions of sea salts and relating salts in each aerosol particle

25   Figure 8 depicts EDX spectra of sea-salt particles and sea-salt-related particles in aerosol particles collected over the sea ice. Na, Mg, S, and Cl were identified in aerosol particles in Fig. 8a. Atomic ratios of these elements were similar to the seawater ratio. Therefore, aerosol particles of this type might be identified as sea-salt particles. Although strong peaks of Na and Cl were observed in aerosol particles in Fig. 8b as well as that in Fig. 8a, the Mg peak height increased remarkably. Particles of this type might be Mg-rich sea-salt particles. Mg-rich sea-salt particles were identified also in the lower troposphere at Syowa

30   Station, Antarctica during winter–spring (Hara et al., 2013). Previous studies (Hara et al., 2012, 2013) presented that Mg-rich particles were released from the sea-ice area and that they are associated with sea-salt fractionation. In addition to Mg enrichment, the peak height of K increased relative to the Na peak as presented in Fig. 8c. Figure 8a shows that the peak

heights of K in sea-salt particles with similar ratios to the seawater ratio are very low. Therefore, the particles might be K-rich sea-salt particles. K-rich sea-salt particles were identified also in the boundary layer over Syowa Station, Antarctica during winter–spring (Hara et al., 2013a) and near the surface on the Antarctic plateau during summer (Hara et al., 2014).

5   In addition to enrichment of Mg and K in sea-salt particles, the peak height of Cl decreased relative to Na and Mg in the aerosol particles presented in Fig. 8d. In this particle, Cl-loss might proceed by heterogeneous reactions with acidic species such as NO_3^- and the precursors in polar regions, as discussed by Hara et al. (1999, 2002, 2005, 2013), because of a non-significant increase of the S peak. Because of the presence of strong peaks of C and O, and low sensitivity of N in EDX analysis, the N peak was identified to only a slight degree in this study. Consequently, particles of this type might be the modifying sea-salt
10   particles. For other modifying sea-salt particles, the peak height of Cl decreased concomitantly with the S peak increase (not presented in Fig. 8). Sea-salt modifications are discussed in later sections. Na, Mg, and S were detected from aerosol particles in Fig. 8e. Because of absence of a Cl peak and very weak S peak, this particle might be identified as the wholly Cl-depleted sea-salt particles with NO_3^-. Here, we designate wholly Cl-depleted sea-salt particles as "modified sea-salt particles." Partly Cl-depleted sea-salt particles were classified as "sea-salt particles."

       Actually, Si, Al, Ca, and Fe were detected in some sea-salt particles and modified sea-salt particles (Fig. 8f). Because Si and Al are major elements of minerals, the particle in Fig. 8f might be internal mixture of sea salts and minerals. Strong peaks of Na and S were identified from the coarse particle in Fig. 8g. Because Mg ratios in coarse sea-salt particles exceed the usual detection limit of single particle analysis by EDX, the aerosol particles might have an extremely poor Mg ratio. For this study,
20   particles of this type are designated as "Mg-free" particles. The atomic ratio of Na and S of the Mg-free particles implies strongly that the particles were in the form of Na_2SO_4. Details of the particles are discussed in a later section. Peaks of Mg and Cl were observed in the particle portrayed in Fig. 8h. Atomic ratios of Mg and Cl of the aerosol particles containing only Mg and Cl were approximately compatible with $MgCl_2$. Also, $MgCl_2$ particles were identified also in the boundary layer at Syowa Station, Antarctica, but only during winter (Hara et al., 2013). Figure S3 shows that Mg might be present as $MgCl_2$ in sea-salt
25   particles. Actually, Mg and S were detected from aerosol particles in Fig. 8i. Atomic ratios of Mg and S of the aerosol particles containing only Mg and S were approximately compatible with $MgSO_4$. Considering that $MgCl_2$ can react with sulphuric acid similarly to Cl modifying and modified sea-salt particles, $MgSO_4$ might be formed through heterogeneous reactions. In addition, $MgSO_4$ particles were observed in the atmosphere at Syowa Station, Antarctica (Hara et al., 2013) and on the Antarctic continent (Hara et al., 2014). In the aerosol particle presented in Fig. 8j, K and Cl were detected clearly. Atomic ratios of K
30   and Cl showed that particles of this type might be composed of KCl. In earlier studies conducted at Syowa Station, Antarctica (Hara et al., 2013), KCl-rich particles were observed only once during the winter.

3.7 Abundance of sea-salt particles and sea-salt-related particles

For quantitative discussion, the relative abundance was estimated from the results of EDX analyses (Fig. 9). In this study, sea-salt and modified sea-salt particles were major components of the coarse mode. Although a few samples showed low relative abundance of sea-salt particles and modified sea-salt particles, this result corresponded to high relative abundance of minerals

5 and minerals containing sulphates. However, it is noteworthy that the low number concentrations in coarse mode in the atmosphere engender low number density on the sample substrates and engender high uncertainty. For number concentrations of less than 10 L^{-1} in D_P> 2.0 μm, the number of the analysed particles in coarse mode was several to approximately 16 particles.

Aerosol particles containing sulphates were dominant in fine mode. Therefore, the relative abundance of sea-salt and modified

10 sea-salt particles was lower in most samples. The relative abundance of sea-salt particles and modified sea-salt particles in fine mode showed higher abundance than 40% under conditions with strong winds or high number concentrations in coarse mode. Although laboratory experiments reported by Roscoe et al. (2011) showed non-significant aerosol release from sea ice with the appearance of frost flowers, the non-significant aerosol release cannot account for the high relative abundance of sea-salt particles or the presence of the fractionated sea-salt particles (i.e., Mg-rich sea-salt particles). Blowing and drifting snow was

15 observed in strong winds during the campaign. Therefore, sea-salt particles might be released remarkably into the atmosphere by the fracture of frost flowers and erosion of snow mixed with brine on the sea ice under the strong winds. Details of sea-salt fractionation are described in a later section. The aerosol number concentrations decreased immediately after strong winds except on DOY = 10–15. The features might result from the rapid exchange of air masses and the rapid deposition of coarse sea-salt particles. Although high number concentrations were observed in both coarse and fine modes on DOY = 10–15, the

20 wind speed was less than 7.5 m s^{-1} at Siorapaluk. Consequently, sea-salt particles might be released not from sea ice around the sampling site, but from sea-ice regions with stronger winds. Then they might be transported to the sampling sites.

3.8 Sea-salt modification of aerosol particles in coarse and fine modes

Figure 10 portrays ternary plots (Na–S–Cl) of sea-salt particles and the modified sea-salt particles. The internal mixture of sea salts and minerals were removed from the ternary plots and discussion in order to avoid misunderstanding of sea-salt

25 modification. Labels of A and B respectively denote atomic ratios of bulk seawater ratios and wholly Cl depleted sea-salt particles by SO_4^{2-}. The black line represents the stoichiometric line. When Cl in sea-salt particles is liberated stoichiometrically by heterogeneous reactions (SO_4^{2-} formation), each sea salt particle is distributed along the stoichiometric line.

Coarse sea-salt particles collected near new sea ice (Site III) in DOY = 61.61 (3 March, 2014) were classified into (1) sea-salt

30 particles distributed around bulk seawater ratio and (2) aerosol particles distributed around Na_2SO_4 ratio. Frost flowers had not been formed on a new sea-ice surface on 3 March. Although strong winds were observed in DOY = 58.9–60.3 (28 February – 1 March, 2014) and although they lead to the appearance of an open sea surface by break and flow of sea ice, the wind speed

dropped to less than 2 m s^{-1} in DOY = 60.8 (end of 1 March). Therefore, new sea ice might be formed within one day. The sampling site on 3 March was close to the open sea area and floating sea ice. Therefore, release from the sea surface might account for the presence of sea-salt particles with the bulk seawater ratio. The presence of aerosol particles with Na$_2$SO$_4$ ratio, however, cannot be explained by their release from the sea surface. If the sea-salt particles were modified with SO$_4^{2-}$ by

5 heterogeneous reactions, then the modified sea-salt particles contained sea-salt Mg. Nevertheless, Mg was not detected in the aerosol particles having ratios similar to Na$_2$SO$_4$, as presented in Fig. 8g and Fig. S4. Consequently, the Mg-free sulphate particles might not be the modified sea-salt particles. In the initial stage of sea-ice formation, ikaite (CaCO$_3$ 6H$_2$O) and mirabilite (Na$_2$SO$_4$ 10H$_2$O) are precipitated respectively at -2°C and -8.8 °C on/in sea ice (Dieckmann et al., 2008, 2010; Marion et al., 1999). Additionally, aerosol particles with atomic ratios similar to ikaite or CaCO$_3$ were observed in same aerosol

10 samples (shown in *Supplementary Materials*, Fig. S5). These particles were observed only in aerosol samples collected near new sea ice in this study. Therefore, aerosol particles having atomic ratios similar to Na$_2$SO$_4$ and CaCO$_3$ might be released from new sea ice, in spite of calm winds on 2–3 March. At the moment, release processes of mirabilite-like and ikaite-like particles from the sea-ice surface without frost flowers remain unknown. In contrast, Na-S-Cl ratios in fine sea-salt particles were varied largely in fine mode on 3 March. Modifying sea-salt particles had S ratios lower than the stoichiometric line

15 between bulk seawater and Na$_2$SO$_4$. The modifying sea-salt particles might be modified not only with SO$_4^{2-}$ but also with other acids such as NO$_3^-$, as presented by Hara et al. (1999, 2002, 2005, 2013). Although many aerosol particles in fine mode were distributed around the ratio of Na$_2$SO$_4$, most of the particles contained Mg. Therefore, most of the aerosol particles around Na$_2$SO$_4$ ratio in fine mode might be the modified sea-salt particles by heterogeneous reactions with nss-SO$_4^{2-}$. Because of mixing of nss-SO$_4^{2-}$ in modifying and modified sea-salt particles, direct evidence of sulphate depletion by mirabilite

20 precipitation is only slightly identified in sea-salt and modified sea-salt particles.

Coarse sea-salt particles collected over young sea-ice areas (near Site I) with frost flowers (e.g., on 14 January and 21 February as shown in Figs. 10b–10c) were also distributed around the bulk seawater ratio. Some sea-salt particles had lower Na ratio and higher Cl ratio than the bulk seawater ratio. Mg was enriched considerably in the aerosol particles with lower Na ratios.

25 Details of Mg enrichment are discussed in a later section herein. Similarly to the sample on 3 March, ratios of sea-salt particles in fine mode were varied largely. Sea-salt and modifying sea-salt particles in fine mode on 14 January were distributed around bulk seawater ratios and along with the stoichiometric line. Fine particles collected on 21 February were distributed around the stoichiometric line and Cl ratio = 0. Because of the presence of Mg in fine aerosol particles shown in Figs. 10b–10c, aerosol particles with Cl ratio = 0 might be not mirabilite particles but modified sea-salt particles. Considering the distribution along

30 with the stoichiometric line, sea-salt particles were modified with SO$_4^{2-}$ in both cases (Figs. 10b–10c).

Under conditions with storms and blowing or drifting snow, most of the sea-salt particles in both coarse and fine modes were distributed around the bulk sea-water ratio in Na-Cl-S plot on 1 March (Fig. 10d). A similar tendency was observed in other storm conditions. Sea-salt particles can be released from the surfaces of snow, sand, and sea ice through erosion of surface

snow mixed with brine, with the fracture of frost flowers under strong wind conditions. Therefore, most of the sea-salt particles might be released near the sampling site. In other words, "less-aged (fresh)."

3.9 Variations of sea-salt modification of aerosol particles during winter

Figure 11 depicts variations of Cl/Na and S/Na ratios in coarse and fine sea-salt particles. Sea-salt particles internally mixed with mineral particles were excluded, as the figure shows, to avoid misunderstanding of the sea-salt chemistry. The Cl/Na ratios in coarse mode were higher than those in fine mode. Therefore, sea-salt modification (Cl loss) might be most likely to occur in fine mode. A similar tendency was observed in spring in the Arctic (Hara et al., 2003) and Antarctica (Hara et al., 2005, 2013). High Cl/Na ratios and small variance of Cl/Na ratios in both modes corresponded to samples collected under conditions with blowing or drifting snow and strong winds. Under calm wind conditions, Cl/Na ratios in sea-salt particles vary greatly, which implies that sea-salt particles immediately after release from the sea-ice surface were modified, but not significantly. In other words, sea-salt modification (Cl loss) in sea-salt particles might proceed in the atmosphere during aerosol suspension. Although wide variance of Cl/Na ratios in coarse sea-salt particles was identified in early March, this might result from the presence of mirabilite particles in aerosols, as described above. With the decrease of Cl/Na ratios in sea-salt particles, S/Na ratios increased considerably, especially in fine sea-salt particles. As described above, sulphates might contribute greatly to sea-salt modification in this study. Nitrates might contribute to some degree.

3.10 Sea-salt fractionation of aerosol particles in coarse and fine modes

Figure 12 presents ternary plots of sea-salts (Na, Mg, and S) and Mg-rich sulphates in coarse and fine modes. Internal mixtures of sea salts and minerals were excluded from the ternary plots. Labels of A, B, and C respectively denote the bulk seawater ratio, wholly Cl liberated sea-salt particles by SO_4^{2-}, wholly Na replaced sea-salts (close to $MgCl_2$), and sea-salts (close to $MgSO_4$) with wholly Cl liberation SO_4^{2-} and wholly Na replacement to Mg. When the sea-salt particles are modified by sulphates and are not fractionated, they are distributed around the stoichiometric line of A-B. Mg in sea-salt particles can be enriched gradually with sea-salt fractionation by precipitation of mirabilite ($Na_2SO_4 \cdot 10H_2O$) and hydrohalite ($NaCl \cdot 2H_2O$) (Hara et al., 2012). When sea-salt fractionation (replacement between Na and Mg) occurs without sea-salt modification by sulphate, sea-salt particles are distributed around the stoichiometric line of A-C. When sea-salt fractionation and sea-salt modification by sulphate occur stoichiometrically and simultaneously, sea-salt particles are distributed around the stoichiometric line of A-D. Na-Mg-S ratios of frost flowers and brine were distributed around bulk seawater ratio (a), although slight Mg-enrichment was recognized in this study.

The Mg ratios in coarse aerosol particles collected near new sea ice (Site III) on 3 March were distributed mainly around bulk seawater ratio and NaSO4 ratio. Mg was enriched slightly in some sea-salt particles, even in coarse modes. In contrast to the sea-salt particles, Mg-free particles were distributed around Na_2SO_4 ratio, as depicted in Fig. 8g. As described above, these particles distributed around Na_2SO_4 ratio (B) might be mirabilite particles. In fine mode, most of the sea-salt particles were

distributed between the stoichiometric lines between seawater ratio – $MgSO_4$ and seawater – $MgCl_2$. Compared to the Mg ratio in coarse mode, Mg enrichment was obtained remarkably in fine sea-salt particles.

Although most of the sea-salt particles in coarse mode were distributed around the bulk seawater ratio on 14 January and 21
5   February, 2014, some coarse sea-salt particles had strong Mg-enrichment and were distributed around the stoichiometric line of seawater ratio – $MgCl_2$ (Fig. 26b). A few particles showed atomic ratios roughly equal to that of $MgCl_2$. Therefore, Mg might be in the form of $MgCl_2$ without sea-salt modification with acidic species such as SO_4^{2-} during winter (polar night). Similarly, $MgCl_2$ particles were observed only in the winter at Syowa Station, Antarctica (Hara et al., 2013). Similarly to coarse sea-salt particles, Mg enrichment was also identified in fine mode on 14 January and 21 February, 2014. However, Mg-
10 rich sea-salt particles lay approximately midway between stoichiometric lines of seawater ratio-$MgCl_2$ and seawater ratio-$MgSO_4$. Moreover, $MgSO_4$ particles were identified occasionally in this study (e.g., 21 February, 2014). Therefore, this distribution implies that $MgCl_2$ in Mg-rich sea-salt particles was converted gradually to $MgSO_4$ through the heterogeneous reactions with SO_4^{2-}.

15 In contrast to sea-salt particles on 14 January, 21 February, and 3 March, 2014, sea-salt particles in both modes were distributed mostly around the seawater ratio under storm conditions with blowing or drifting snow on 1 March, 2014, although some sea-salt particles in fine mode had slight Mg enrichment. Aerosol sampling site on 1 March was located on windward side of frost flower area. Therefore, we must notice that sea-salt particles collected on 1 March might be released from surface of aged seasonal ice (old ice in Fig. 1) without frost flowers through erosion of surface snow and sea ice.

20 ### 3.11 Variations of Sea-salt fractionation during winter

Figure 13 presents variations of Mg/Na ratios in sea-salt particles. Sea-salt particles internally mixed with mineral particles were excluded from Fig. 13 to avoid misunderstanding of the sea-salt chemistry. Mg/Na ratios were higher than the bulk seawater ratio (Mg/Na ≈ 0.11) in coarse and fine sea-salt particles during measurements. In conditions with blowing or drifting snow and strong winds, the Mg/Na ratios and the standard deviation decreased in both modes. However, higher Mg/Na ratios
25 were observed in the calm wind conditions. Furthermore, Mg/Na ratios in coarse sea-salt particles increased gradually on DOY = 52–57 (22–27 February), when the air temperature was below -25 °C and the wind speed was lower than 4 m s^{-1}. As presented in Hara et al. (2012), Mg/Na ratios in sea-salt particles had temperature dependence by precipitation of hydrohalite and other salts. Therefore, sea-salt fractionation such as precipitation of hydrohalite might promote higher Mg/Na ratios in coarse sea-salt particles in the coldest conditions. Figure 4 shows that Mg^{2+}/Na^+ ratios in frost flowers at Site I increased gradually on 20
30 February – 1 March. Considering the simultaneous sampling of aerosols and frost flowers at Site I during this period, correspondence between high Mg/Na ratios in coarse mode and the coldest conditions implies strongly that Mg/Na ratios in coarse sea-salt particles responded rapidly to sea-salt fractionation on sea ice and frost flowers. In other words, we must consider the likelihood that sea-salt particles were released from the sea-ice surface and frost flowers under calm wind

conditions, in addition to sea-salt dispersion in strong winds. Considering lower Mg/Na ratios in blowing or drifting snow and strong winds and higher Mg/Na ratios in fine sea-salt particles, higher Mg/Na ratios in calm winds might result from (1) release of Mg-rich sea-salt particles even in weak wind conditions, (2) preferential release of Mg-rich sea-salt particles in fine mode, and (3) efficient deposition of sea-salt particles (probably larger size) without marked Mg-enrichment. Because of a shortage

5 of reliable information about these processes, we discuss only slightly the contribution of each process to the presence of Mg-rich sea-salt particles in the atmosphere.

In contrast to coarse sea-salt particles, Mg/Na ratios were higher in fine modes in this study. Similar tendencies were observed in aerosol particles over Syowa Station, coastal Antarctica (Hara et al., 2013), and on the Antarctic continent (Hara et al.,

10 2014). As discussed in this study and in previous works (Hara et al., 2012, 2013, 2014), Mg enrichment in sea-salt particles was associated with sea-salt fractionation on sea ice and snow. This size dependence of Mg enrichment in sea-salt particles is important to understand the release processes of sea-salt particles from sea ice and frost flowers. The outward contrast might result from heterogeneous distributions of sea salts on and in sea ice, frost flowers, and brine. If sea salts were distributed homogeneously on and in sea ice, frost flowers, and brine, then the size dependence of Mg enrichment might not occur in sea-

15 salt particles released from sea-ice areas. Therefore, high Mg enrichment in fine mode strongly suggests the localization of Mg salts on and in the residual brines, sea ice and frost flowers, and preferential release of fine aerosol particles containing Mg-rich salts from sea ice and frost flowers. To elucidate this point, we must know more about the salt-distribution on and in frost flowers and sea ice at the nanometre – micrometre scale.

4. Concluding remarks

20 Simultaneous sampling and observations of frost flowers, brines, and atmospheric aerosol particles were conducted around Siorapaluk, north-western Greenland at the end of December, 2013 – early March 2014. Sea-salts in frost flowers and brines were concentrated relative to the seawater ratio. Concentration factors of frost flowers and brines were 1.14–3.67. Furthermore, sea-salts (Mg^{2+}, K^+, Ca^{2+}, Cl^-, Br^-, and I) were enriched remarkably in frost flowers with sea-salt fractionation by precipitation of mirabilite and hydrohalite. Molar ratios of sea-salts (Mg^{2+}/Cl^-, K^+/Cl^-, Ca^{2+}/Cl^-, and Br^-/Cl^-) changed gradually with aging

25 and growth of frost flowers under colder conditions. Changes of I/Cl$^-$ ratio in frost flowers, however, were not clear. Br$^-$ and I were liberated from frost flowers through heterogeneous reactions. Liberation from frost flowers might be more likely to proceed relative to Br$^-$ liberation. Considering T_{FF} dropped to -21.3 °C, sea-salt fractionation (mirabilite and hydrohalite precipitation) might be promoted in brine on sea ice. Then, the residual brine might be migrated vertically onto frost flowers. In the atmosphere, Mg was enriched in sea-salt particles. Mg in sea-salt particles was in the form of $MgCl_2$ and $MgSO_4$.

30 Particularly, Mg might be more likely to be enriched in fine mode. Mg enrichment in sea-salt particles was enhanced under colder conditions. In addition, ikaite-like and mirabilite-like particles identified in the atmosphere only near new sea ice are close to the sea-ice margin.

Acknowledgments

We would like to thank Ikuo Oshima and residents at Siorapaluk for extremely useful comments and help related to operations on sea ice, sea-ice conditions, and appearance of frost flowers. This study was supported by a Grant-in-Aid for Challenging Exploratory Research (PI: K. Hara, No. 25550018).

5 **References**

Abbatt, J., Thomas, J., Abrahamsson, K., Boxe, C., Granfors, A., Jones, A., King, M., Saiz-Lopez, A., Shepson, P., Sodeau, J., Toohey, D., Toubin, C., Glasow, R., Wren, S., and Yang, X.: Halogen activation via interactions with environmental ice and snow in the polar lower troposphere and other regions, Atmospheric Chemistry and Physics, 12, doi:10.5194/acp-12-6237-2012, 2012.

10 Alvarez-Aviles, L., Simpson, W., Douglas, T., Sturm, M., Perovich, D., and Domine, F.: Frost flower chemical composition during growth and its implications for aerosol production and bromine activation, Journal of Geophysical Research, doi:10.1029/2008JD010277, 2008.

Barrie, L. A., Bottenheim, J. W., Schnell, R. C., and Crutzen, P. J.: Ozone destruction and photochemical reactions at polar sunrise in the lower Arctic atmosphere, Nature, 334, 138–141, doi:10.1038/334138a0, 1988.

15 Carpenter, L. J.: Iodine in the marine boundary layer, Chem. Rev., 103(12), 4953–4962, doi:10.1021/cr0206465, 2003.

Chen, Z., Megharaj, M., and Naidu, R.: Speciation of iodate and iodide in seawater by non-suppressed ion chromatography with inductively coupled plasma mass spectrometry, Talanta, 72(5), 1842–1846, doi:10.1016/j.talanta.2007.02.014, 2007.

Dieckmann, G. S., Nehrke, G., Papadimitriou, S., Göttlicher, J., Steininger, R., Kennedy, H., Wolf-Gladrow, D., and Thomas, D. N.: Calcium carbonate as ikaite crystals in Antarctic sea ice, Geophysical Research Letters, 35(8),
20 doi:10.1029/2008GL033540, 2008.

Dieckmann, G., Nehrke, G. Uhlig, C., and Göttlicher, J: Ikaite ($CaCO_3\bullet 6H_2O$) discovered in Arctic sea ice, The Cryosphere, doi:10.5194/tc-4-227-2010, 2010.

Ding, Z. J., Li, Y. G., Zeng, R. G., Mao, S. F., Zhang, P., and Zhang, Z. M.: Depth distribution functions of secondary electron production and emission, J. Surface Anal., 15, 249–253, 2009.

25 Domine, F., Taillandier, A., Simpson, W., and Severin, K.: Specific surface area, density and microstructure of frost flowers, Geophysical Research Letters, 32(13), doi:10.1029/2005GL023245, 2005

Douglas, T., Domine, F., Barret, M., Anastasio, C., Beine, H., Bottenheim, J., Grannas, A., Houdier, S., Netcheva, S., Rowland, G., Staebler, R., and Steffen, A.: Frost flowers growing in the Arctic Ocean – atmosphere – sea ice – snow interface: 1. Chemical composition, Journal of Geophysical Research, 117, doi:10.1029/2011JD016460, 2012.

30 Ebinghaus, R., Kock, H., Temme, C., Einax, J., Löwe, A., Richter, A., Burrows, J., and Schroeder, W.: Antarctic Springtime Depletion of Atmospheric Mercury, Environmental Science & Technology, 36(6), 1238–1244, doi:10.1021/es015710z, 2002.

Foster, K. L., Plastridge, R. A., Bottenheim, J. W., Shepson, P. B., Finlayson-Pitts, B. J., and Spicer, C. W.: The role of Br2 and BrCl in surface ozone destruction at polar sunrise., Science, 291(5503), 471–474, doi:10.1126/science.291.5503.471, 2001.

Geilfus, N.-X., Galley, R., Cooper, M., Halden, N., Hare, A., Wang, F., Søgaard, D., and Rysgaard, S.: Gypsum crystals observed in experimental and natural sea ice, Geophysical Research Letters, doi:10.1002/2013GL058479, 2013.

Goldstein, J. I., Newbury, D. E., Joy, D. C., Lyman, C. E., Echlin, P., Lifshin, E., Sawyer, L., and Michael, J.: Chapter 6 Generation of X-rays in the SEM specimen, in: Scanning Electron Microscopy and X-ray Micronalysis, 3, 271–296, Plenum Press, New York, 2003.

Hara, K., Nakazawa, F., Fujita, S., Fukui, K., Enomoto, H., and Sugiyama, S.: Horizontal distributions of aerosol constituents and their mixing states in Antarctica during the JASE traverse, Atmospheric Chemistry and Physics, 14(18), 10211–10230, doi:10.5194/acp-14-10211-2014, 2014.

Hara, K., Osada, K., Hayashi, M., Matsunaga, K., Shibata, T., Iwasaka, Y., and Furuya, K.: Fractionation of inorganic nitrates in winter Arctic troposphere: Coarse aerosol particles containing inorganic nitrates, Journal of Geophysical Research, doi:10.1029/1999JD900348, 1999.

Hara, K., Osada, K., Kido, M., Hayashi, M., Matsunaga, K., Iwasaka, Y., Yamanouchi, T., Hashida, G., and Fukatsu, T.: Chemistry of sea-salt particles and inorganic halogen species in Antarctic regions: Compositional differences between coastal and inland stations, Journal of Geophysical Research, 109(D20), doi:10.1029/2004JD004713, 2004.

Hara, K., Osada, K., Kido, M., Matsunaga, K., Iwasaka, Y., Hashida, G., and Yamanouchi, T.: Variations of constituents of individual sea-salt particles at Syowa Station, Antarctica, Tellus B, 57(3), 230–246, doi:10.1111/j.1600-0889.2005.00142.x, 2005.

Hara, K., Osada, K., Yabuki, M., and Yamanouchi, T.: Seasonal variation of fractionated sea-salt particles on the Antarctic coast, Geophysical Research Letters, 39(18), doi:10.1029/2012GL052761, 2012.

Hara, K., Osada, K., and Yamanouchi, T.: Tethered balloon-borne aerosol measurements: seasonal and vertical variations of aerosol constituents over Syowa Station, Antarctica, Atmospheric Chemistry and Physics, 13(17), 9119–9139, doi:10.5194/acp-13-9119-2013, 2013.

Hirokawa, T., Ichihara, T., Ito, K., and Timerbaev, A.: Trace ion analysis of seawater by capillary electrophoresis: determination of iodide using transient isotachophoretic preconcentration, Electrophoresis, 24(14), 2328–2334, doi:10.1002/elps.200305445, 2003.

Horikawa, Y., Kusumoto, R., Yamane, K., Nomura, R., Hirokawa, T., and Ito, K.: Determination of Inorganic Anions in Seawater Samples by Ion Chromatography with Ultraviolet Detection Using Monolithic Octadecylsilyl Columns Coated with Dodecylammonium Cation, Analytical Sciences, 32(10), 1123–1128, doi:10.2116/analsci.32.1123, 2016.

Ito, K.: Determination of Iodide in Seawater by Ion Chromatography, Analytical Chemistry, 69(17), 3628–3632, doi:10.1021/ac9700787, 1997.

Ito, K.: Semi-micro ion chromatography of iodide in seawater, Journal of Chromatography A, 830(1), 211–217, doi:10.1016/S0021-9673(98)00910-8, 1999.

Ito, K., Ichihara, T., Zhuo, H., Kumamoto, K., Timerbaev, A., and Hirokawa, T.: Determination of trace iodide in seawater by capillary electrophoresis following transient isotachophoretic preconcentration Comparison with ion chromatography, Analytica Chimica Acta, 497(1-2), 67–74, doi:10.1016/j.aca.2003.08.052, 2003

Jungwirth, P. and Tobias, D.: Molecular Structure of Salt Solutions: A New View of the Interface with Implications for Heterogeneous Atmospheric Chemistry, Journal of Physical Chemistry B, doi:10.1021/jp012750g, 2001.

Kaleschke, L., Richter, A., Burrows, J., Afe, O., Heygster, G., Notholt, J., Rankin, A., Roscoe, H., Hollwedel, J., Wagner, T., and Jacobi, H. W.: Frost flowers on sea ice as a source of sea salt and their influence on tropospheric halogen chemistry, Geophysical Research Letters, 31(16), doi:10.1029/2004GL020655, 2004.

Kelly, J. and Wexler, A.: Thermodynamics of carbonates and hydrates related to heterogeneous reactions involving mineral aerosol, Journal of Geophysical Research, doi:10.1029/2004JD005583, 2005.

Koop, T., Kapilashrami, A., Molina, L., and Molina, M.: Phase transitions of sea-salt/water mixtures at low temperatures: Implications for ozone chemistry in the polar marine boundary layer, Journal of Geophysical Research, 105(D21), 26393, doi:10.1029/2000JD900413, 2000.

Lide, D. R., Handbook of Chemistry and Physics 86th edition, 2005.

Marion, G., Farren, R., and Komrowski, A.: Alternative pathways for seawater freezing, Cold Regions Science and Technology, 29(3), 259266, doi:10.1016/S0165-232X(99)00033-6, 1999.

Martin, S., Drucker, R., and Fort, M.: A laboratory study of frost flower growth on the surface of young sea ice, Journal of Geophysical Research: Oceans (1978–2012), 100(C4), doi:10.1029/94JC03243, 1995.

Martin, S., Yu, Y., and Drucker, R.: The temperature dependence of frost flower growth on laboratory sea ice and the effect of the flowers on infrared observations of the surface, Journal of Geophysical Research: Oceans, 1978 2012, 101(C5), doi:10.1029/96JC00208, 1996.

Millero, F., Feistel, R., Wright, D., and McDougall, T.: The composition of Standard Seawater and the definition of the Reference-Composition Salinity Scale, Deep Sea Research Part I: Oceanographic Research Papers, 55(1), 50–72, doi:10.1016/j.dsr.2007.10.001, 2008

Mochida, M., Hirokawa, J., and Akimoto, H.: Unexpected large uptake of O_3 on sea salts and the observed Br_2 formation, Geophysical Research Letters, 27(17), 2629–2632, doi:10.1029/1999GL010927, 2000.

Obbard, R., Roscoe, H., Wolff, E., and Atkinson, H.: Frost flower surface area and chemistry as a function of salinity and temperature, Journal of Geophysical Research, doi:10.1029/2009JD012481, 2009.

Perovich, D. and Richter-Menge, J.: Surface characteristics of lead ice, Journal of Geophysical Research: Oceans (1978–2012), 99(C8), doi:10.1029/94JC01194, 1994.

Rankin, A., Auld, V., and Wolff, E.: Frost flowers as a source of fractionated sea salt aerosol in the polar regions, Geophys. Res. Lett., doi:10.1029/2000GL011771, 2000.

Rankin, A., Wolff, E. and Martin, S.: Frost flowers: Implications for tropospheric chemistry and ice core interpretation, Journal of Geophysical Research, 107(D23), doi:10.1029/2002JD002492, 2002.

Roscoe, H., Brooks, B., Jackson, A., Smith, M., Walker, S., Obbard, R., and Wolff, E.: Frost flowers in the laboratory: Growth, characteristics, aerosol, and the underlying sea ice, Journal of Geophysical Research, doi:10.1029/2010JD015144, 2011.

5 Saiz-Lopez, A., Blaszczak-Boxe, C., and Carpenter, L.: A mechanism for biologically induced iodine emissions from sea ice, Atmos. Chem. Phys., 15(17), 9731–9746, doi:10.5194/acp-15-9731-2015, 2015.

Schroeder, W. H., Anlauf, K. G., Barrie, L. A., Lu, J. Y., and Steffen, A.: Arctic springtime depletion of mercury, Nature, 394, 331-332, 1998.

Simpson, W., Alvarez-Aviles, L., Douglas, T., Sturm, M., and Domine, F.: Halogens in the coastal snow pack near Barrow,
10   Alaska: Evidence for active bromine air–snow chemistry during springtime, Geophysical Research Letters, 32(4), doi:10.1029/2004GL021748, 2005.

Simpson, W. R., von Glasow, R., Riedel, K., Anderson, P., Ariya, P., Bottenheim, J., Burrows, J., Carpenter, L. J., Frieß, U., Goodsite, M. E., Heard, D., Hutterli, M., Jacobi, H.-W., Kaleschke, L., Neff, B., Plane, J., Platt, U., Richter, A., Roscoe, H., Sander, R., Shepson, P., Sodeau, J., Steffen, A., Wagner, T., and Wolff, E.: Halogens and their role in polar boundary-
15   layer ozone depletion, Atmos. Chem. Phys., 7, 4375-4418, doi:10.5194/acp-7-4375-2007, 2007.

Style, R. and Worster, M.: Frost flower formation on sea ice and lake ice, Geophysical Research Letters, doi:10.1029/2009GL037304, 2009.

Thompson, A. M. and Zafiriou, O. C.: Air-Sea Fluxes of Transient Atmospheric Species, J. Geophys. Res., 88, 6696–6708, doi:10.1029/JC088iC11p06696, 1983.

20 Udisti, R., Dayan U., Becagli S., Busetto M., Frosini D., Legrand M., Lucarelli F., Preunkert S., Severi M., Traversi R., and Vitale V.: Sea spray aerosol in central Antarctica. Present atmospheric behaviour and implications for paleoclimatic reconstructions, Atmos. Environ., 52, 109–120, 2012.

Wagenbach, D., Ducroz, F., Mulvaney, R., Keck, L., Minikin, A., Legrand, M., Hall, J., and Wolff, E.: Sea-salt aerosol in coastal Antarctic regions, Journal of Geophysical Research, doi:10.1029/97JD01804, 1998.

25 Wolff, E., Fischer, H., Fundel, F., Ruth, U., Twarloh, B., Littot, G., Mulvaney, R., Röthlisberger, R., de Angelis, M., Boutron, C., Hansson, M., Jonsell, U., Hutterli, M., Lambert, F., Kaufmann, P., Stauffer, B., Stocker, T., Steffensen, J., Bigler, M., Siggaard-Andersen, M., Udisti, R., Becagli, S., Castellano, E., Severi, M., Wagenbach, D., Barbante, C., Gabrielli, P., and Gaspari, V.: Southern Ocean sea-ice extent, productivity and iron flux over the past eight glacial cycles, Nature, 440, 491–496, doi:10.1038/nature04614, 2006.

30 Wolff, E. W., Rankin, A. M., and Röthlisberger, R.: An ice core indicator of Antarctic sea ice production, Geophys. Res. Lett., 30(22), 2158, doi:10.1029/2003GL018454, 2003.
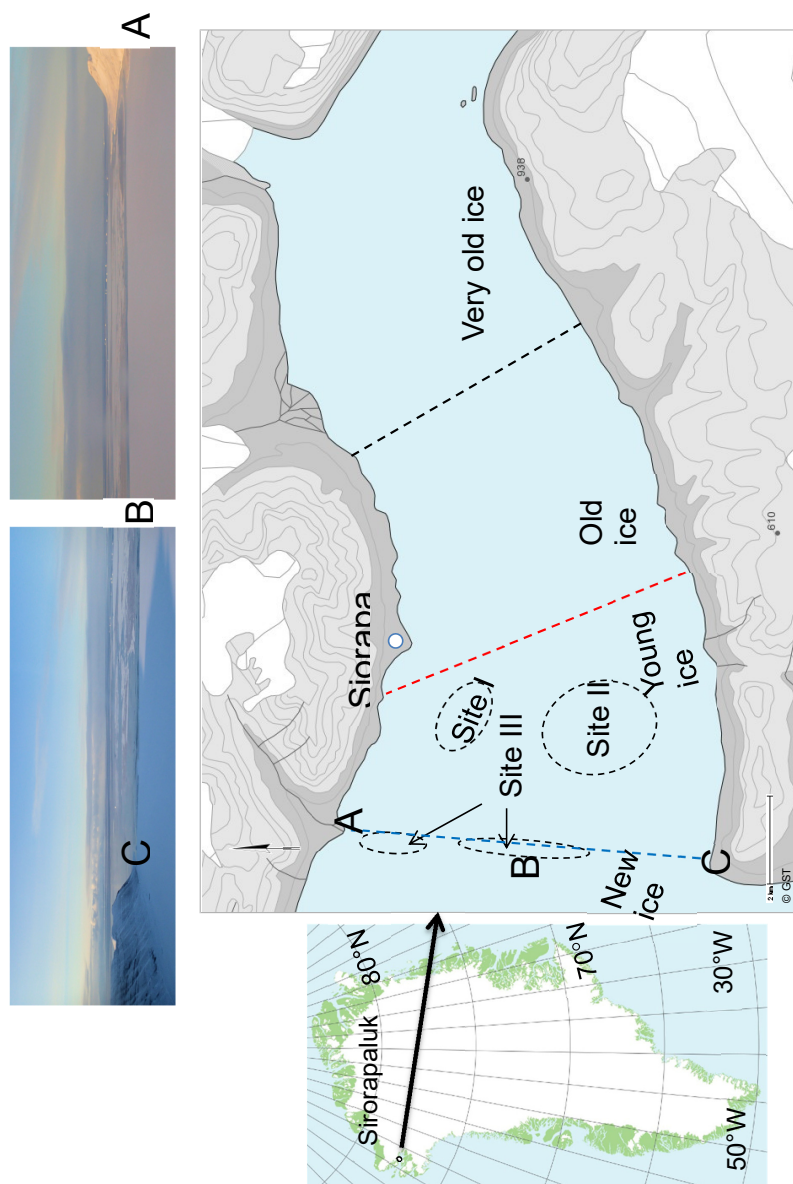
Figure 1 Locations of sampling and sea-ice conditions around Siorapaluk and photographs of new sea-ice conditions off Siorapaluk (taken from helicopter on 7 March, 2014). Broken lines show locations of sea-ice break. Marks of A, B, and C denote broad locations in maps and photographs.
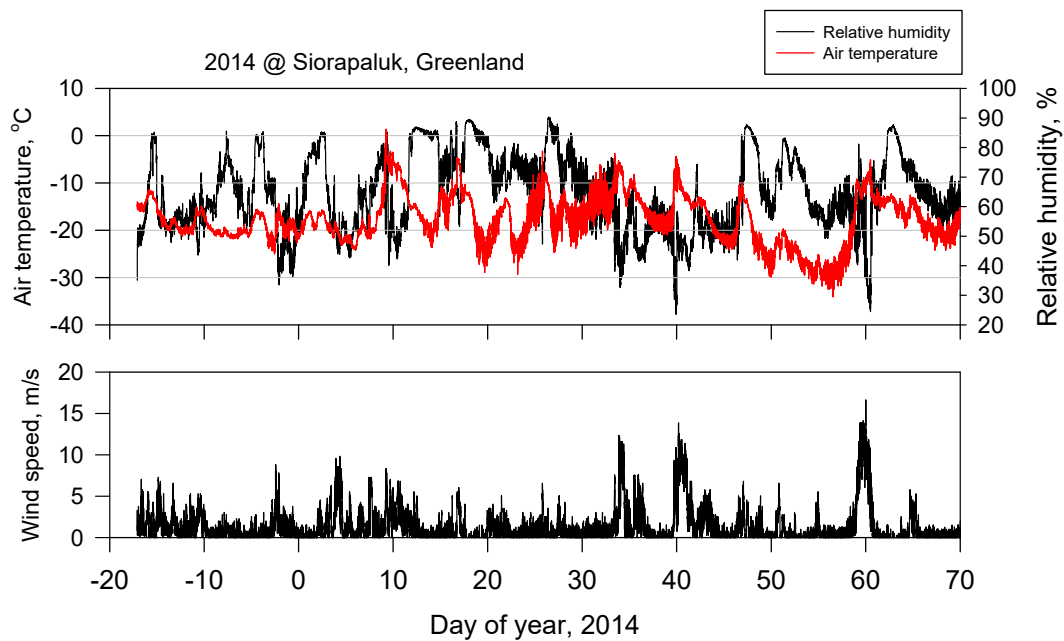
Figure 2 Variation of air temperature, relative humidity, and wind speed at Siorapaluk.

Fig.3
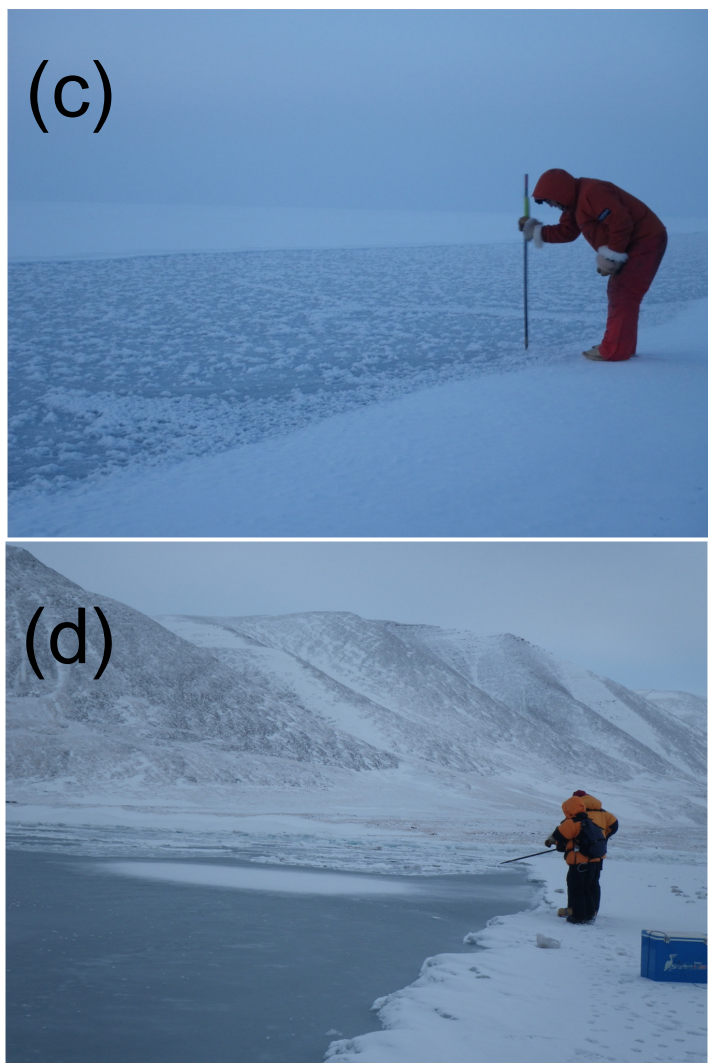
Fig.3

Figure 3 Photographs of (a) frost flowers at Site I, (b) frost flowers on 22 February at Site I, (c) frost flowers at Site II, and (d) frost flowers on 4 March at Site III
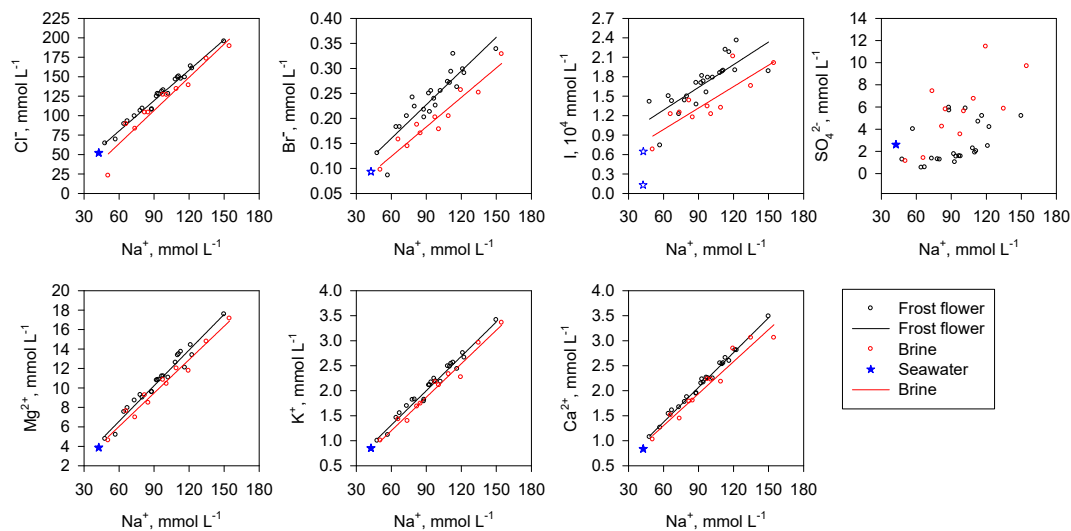
Figure 4 Relation among each constituent to Na⁺ concentration of frost flowers, brine, and seawater taken in this study. Black and red lines respectively present regression lines of frost flowers and brine. Open black and red circles respectively present concentrations in frost flowers and brine. Filled blue stars represent the concentrations of seawater taken around Siorapaluk. Open blue stars represent the concentrations of seawater in the literature presented in Table 1.
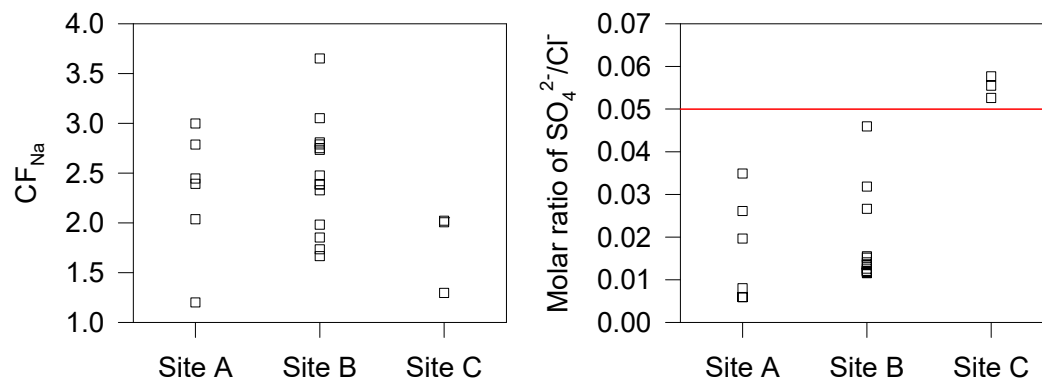
Figure 5 Variations of (a) concentration factor of Na⁺ (CF$_{Na}$) and (b) molar ratios of SO$_4^{2-}$/Na⁺ in frost flowers at each sampling site.
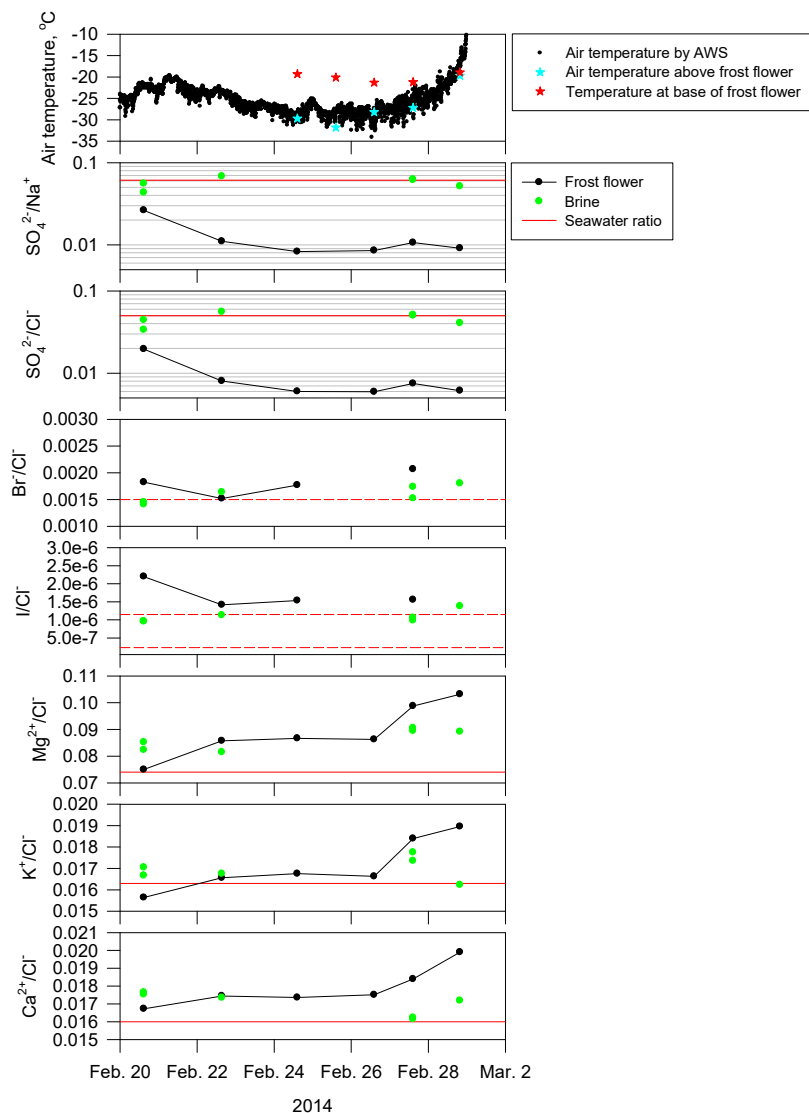
Figure 6 Short-term features of (a) air temperature measured by AWS (T$_{AWS}$), air temperature above frost flowers (T$_{air}$, ca. 10 cm above the sea-ice surface), temperature of base of frost flowers (T$_{FF}$), and (b–h) molar ratios of sea-salts in frost flowers and brine at Site I. T$_{air}$ and T$_{FF}$ were not measured on 20–22 February.
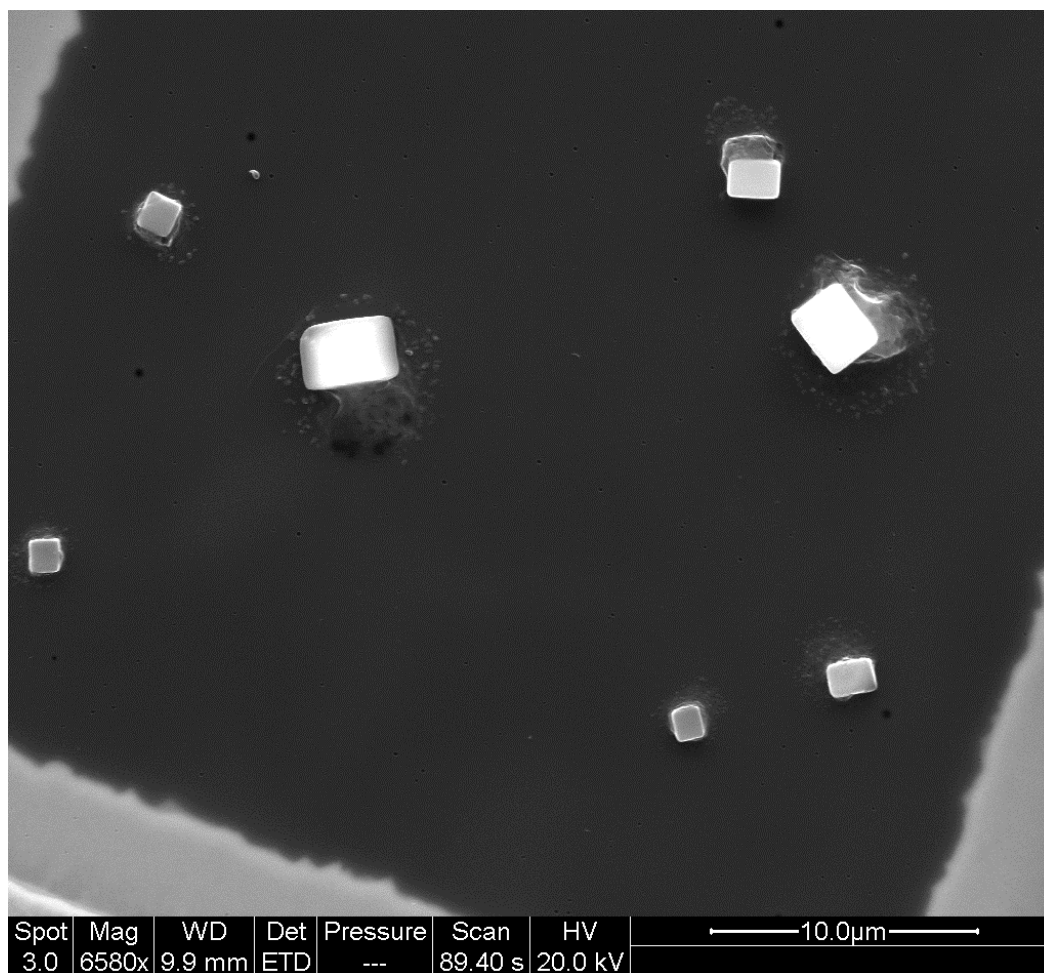
Figure 7 SEM image of aerosol particles collected on 1 March, 2014 above the sea-ice area with frost flowers.
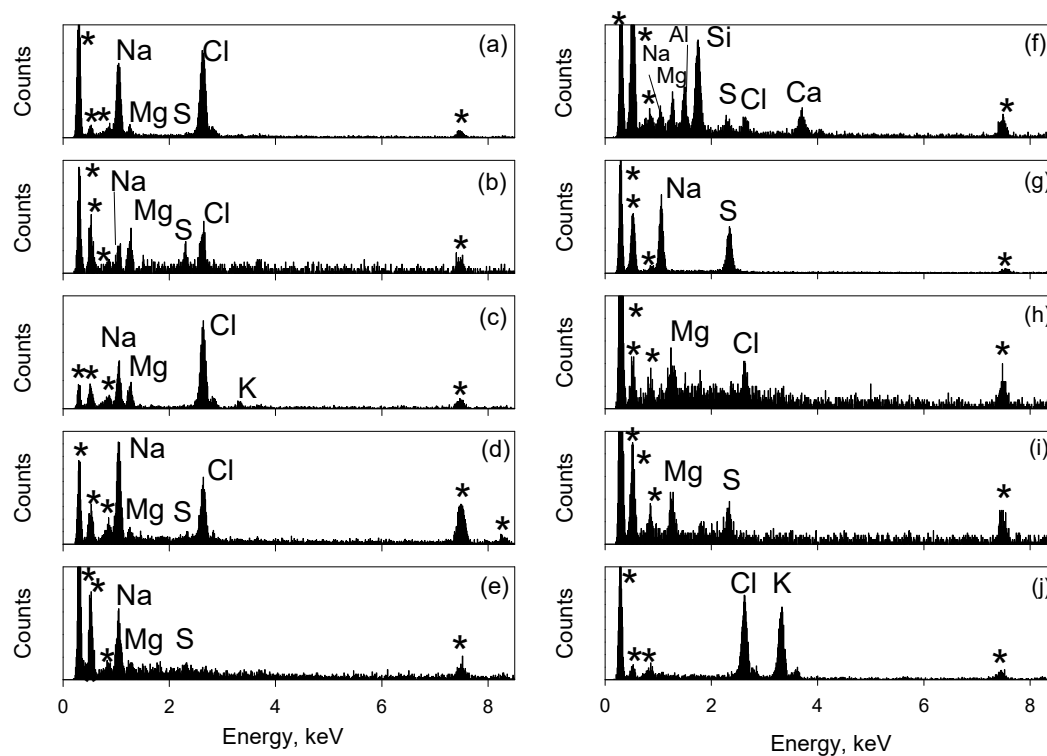
Figure 8 EDX spectra of sea-salt particles and sea-salt relating particles collected over the sea-ice area.
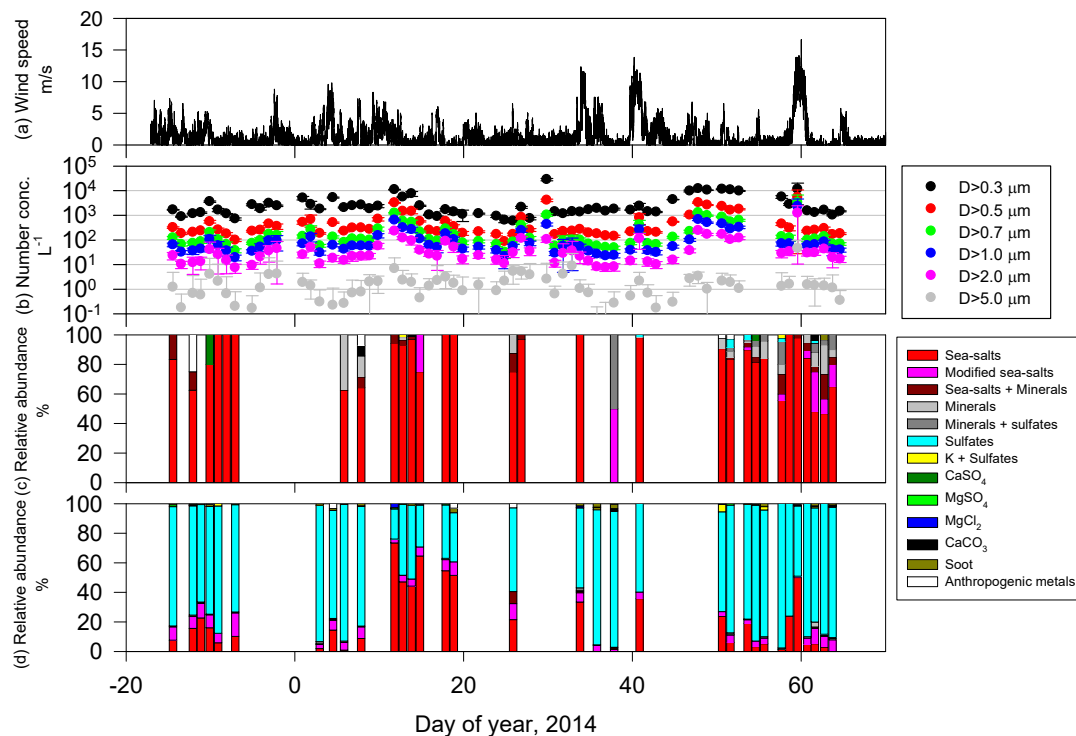
Figure 9 Variations of wind speed, aerosol number concentrations, relative abundance of each aerosol type in coarse and fine modes.
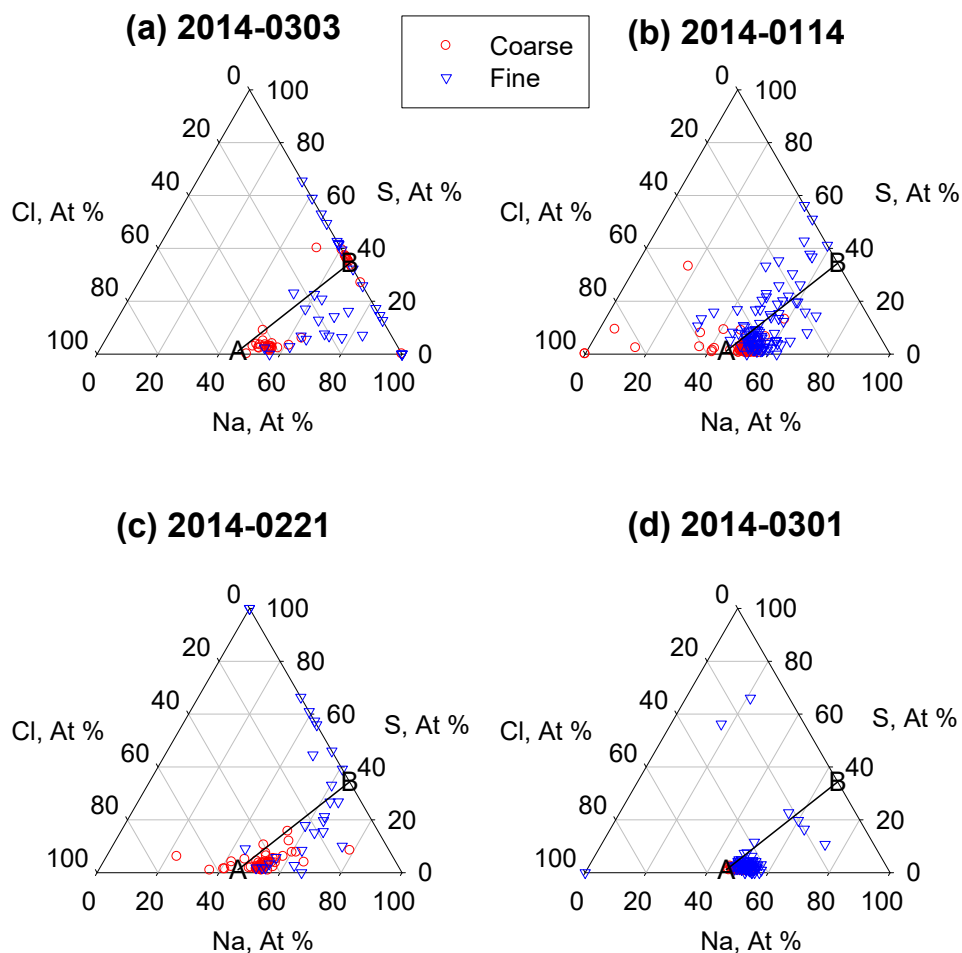
Figure 10 Ternary plots of Na–S–Cl of sea-salt particles and the modified sea-salt particles collected over the sea-ice area. A and B in this figure respectively denote ratios of seawater and fully modified with SO_4^{2-}. Red open circles and blue triangles respectively present ratios of each particle in coarse and fine modes.
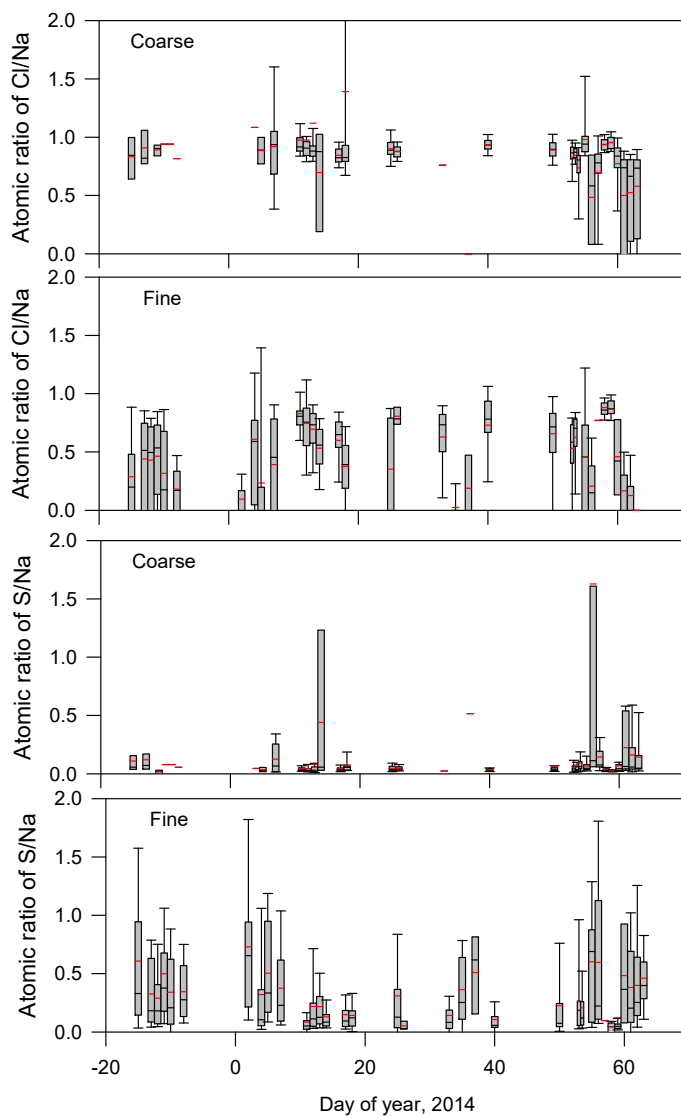
Figure 11 Variations of atomic ratios of Cl/Na and S/Na in sea-salt particles and the modified sea-salt particles collected over the sea-ice area. In box plots, the top bar, top box line, black middle box line, bottom box line, and bottom bar respectively show values of 90, 75, 50 (median), 25, and 10%. The red line shows mean values.
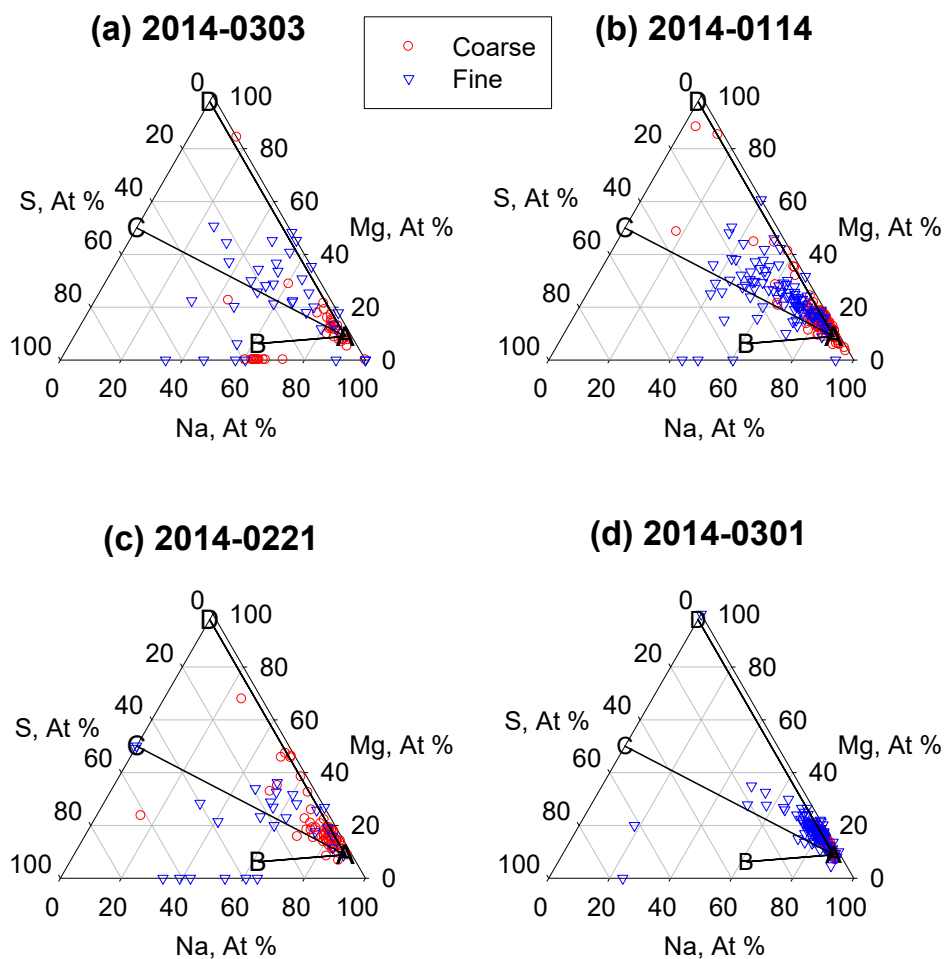
Figure 12 Ternary plots of Na–Mg–S of sea-salt particles and the modified sea-salt particles collected over the sea-ice area. A, B, C, and D in this figure denote ratios of seawater, fully modified respectively with SO$_4^{2-}$, MgSO$_4$, and MgCl$_2$. Red open circles and blue triangles respectively present ratios of particles in coarse and fine modes.
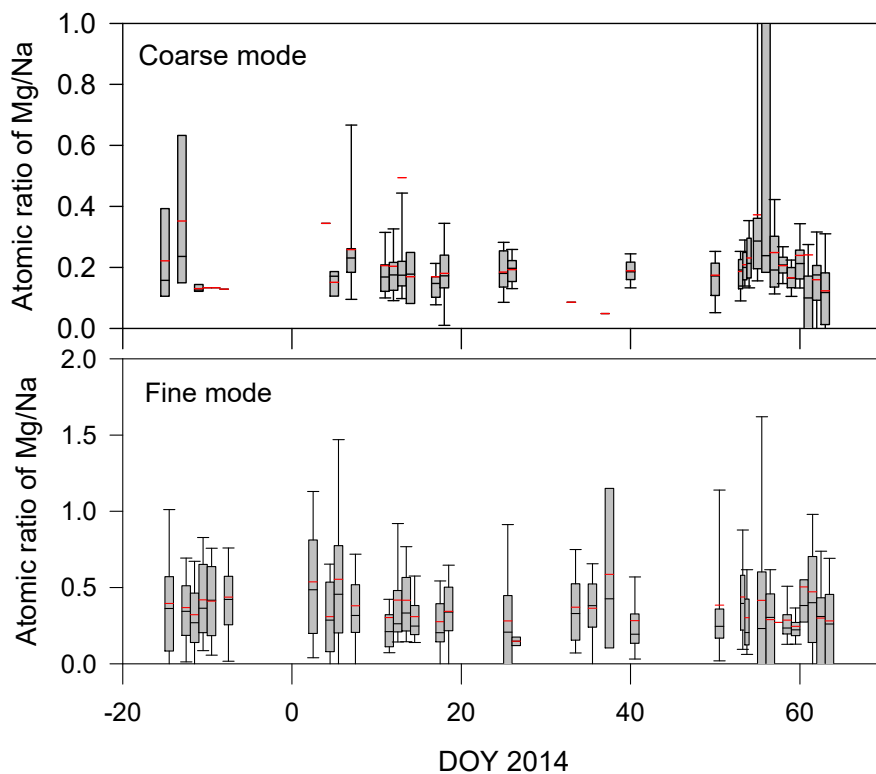
Figure 13 Variations of atomic ratios of Mg/Na in sea-salt particles and the modified sea-salt particles collected over the sea-ice area. In box plots, the top bar, top box line, black middle box line, bottom box line, and bottom bar respectively denote values of 90, 75, 50 (median), 25, and 10%. The red line shows mean values.

Table 1 Statics of molar ratios of sea-salts relative to Na$^+$ and Cl$^-$ concentrations in frost flower, brine and seawater collected in this study ("n" indicates sample number).

		K$^+$/Na$^+$	Mg^{2+}/Na$^+$	Ca^{2+}/Na$^+$	Cl$^-$/Na$^+$	SO$_4^{2-}$/Na$^+$	Br$^-$/Na$^+$	I/Na$^+$	K$^+$/Cl$^-$	Mg^{2+}/Cl$^-$	Ca^{2+}/Cl$^-$	SO$_4^{2-}$/Cl$^-$	Br$^-$/Cl$^-$	I/Cl$^-$
Frost flower n=23	Ave	0.022	0.113	0.023	1.326	0.0288	0.0025	1.83×10^{-6}	0.017	0.086	0.017	0.0223	0.0019	1.38×10^{-6}
	STD	0.001	0.008	0.001	0.052	0.0195	0.0003	3.38×10^{-7}	0.000	0.004	0.000	0.0162	0.0002	2.42×10^{-7}
	median	0.023	0.116	0.023	1.351	0.0190	0.0025	1.83×10^{-6}	0.017	0.086	0.017	0.0141	0.0019	1.35×10^{-6}
	min	0.020	0.091	0.022	1.217	0.0082	0.0015	1.26×10^{-6}	0.016	0.074	0.017	0.0059	0.0012	9.65×10^{-7}
	max	0.023	0.121	0.024	1.387	0.0701	0.0031	2.95×10^{-6}	0.017	0.093	0.018	0.0576	0.0023	2.20×10^{-6}
Brine n=11	Ave	0.021	0.105	0.022	1.170	0.0562	0.0020	1.46×10^{-6}	0.019	0.096	0.020	0.0491	0.0019	1.35×10^{-6}
	STD	0.001	0.008	0.001	0.246	0.0260	0.0002	2.47×10^{-7}	0.008	0.035	0.008	0.0216	0.0008	5.77×10^{-7}
	median	0.021	0.109	0.022	1.230	0.0557	0.0020	1.37×10^{-6}	0.017	0.085	0.017	0.0489	0.0017	1.13×10^{-6}
	min	0.019	0.091	0.020	0.451	0.0210	0.0018	1.21×10^{-6}	0.016	0.081	0.016	0.0156	0.0014	9.56×10^{-7}
	max	0.022	0.115	0.024	1.346	0.1006	0.0024	1.85×10^{-6}	0.044	0.202	0.045	0.0891	0.0043	2.97×10^{-6}
Seawater n=2		0.020	0.091	0.020	1.227	0.0613	0.0018 [a]	$2.76 \times 10^{-7} \sim 1.37 \times 10^{-6}$ [b]	0.016	0.074	0.016	0.0500	0.0015 [a]	$2.32 \times 10^{-7} \sim 1.15 \times 10^{-6}$ [b]

a) Molar ratios of Br$^-$ were listed using bulk seawater ratio (Lide, 2005).

b) Iodine (I$^-$ + IO$_3^-$) concentration in seawater was estimated from the concentrations of I$^-$ and IO$_3^-$ measured by Ito (1997, 1999), Hirooka et al., (2003), Ito et al. (2003), Chen et al. (2007), and Horikawa et al. (2016). The estimated iodine concentrations in seawater are 0.130 - 0.647 μmol L^{-1}. Upper and lower molar ratios of I/Na and I/Cl were calculated using the estimated iodine concentrations and the concentrations of N$^+$ and Cl$^-$ by Lide (2005).